https://doi.org/10.5194/egusphere-2026-990
Preprint. Discussion started: 5 March 2026

Validation of ceilometer aerosol profile retrievals using sun–sky photometer and balloon-borne in situ measurements

Jorge Muñiz-Rosado[1,2], Alberto Cazorla[1,2], Eric Sauvageat[3], Alexander Haefele[3], Celia Herrero del Barrio[4,5], Ramiro González[4,5], Roberto Román[4,5], Pedro Luis Molina-Molero[1,2], Arlett Díaz-Zurita[1,2], Víctor Manuel Naval-Hernández[1,2], Onel Rodríguez-Navarro[1,2], María José Granados-Muñoz[1,2], Juan Antonio Bravo-Aranda[1,2], Milagros Herrera[6], Daniel Pérez-Ramírez[1,2], Lionel Doppler[7], Lucas Alados-Arboledas[1,2], and Francisco Navas-Guzmán[1,2]

[1]Andalusian Institute for Earth System Research (IISTA-CEAMA), Granada, 18071, Spain
[2]Applied Physics Department, University of Granada, Granada 18071, Spain
[3]Federal Office of Meteorology and Climatology MeteoSwiss, Payerne, 1530, Switzerland
[4]Group of Atmospheric Optics (GOA-UVa), Universidad de Valladolid, 47011, Valladolid, Spain
[5]Laboratory of Disruptive Interdisciplinary Science (LaDIS), 47011, Valladolid, Spain
[6]GRASP SAS, Lille, France
[7]Meteorologisches Observatorium Lindenberg – Richard-Assmann-Observatory (MOL-RAO), Deutscher Wetterdienst (DWD), 15848 Tauche, Germany

Correspondence: Francisco Navas-Guzmán (fguzman@ugr.es)

Abstract.

This study evaluates two approaches for retrieving aerosol properties from ceilometer observations, using aerosol optical depth (AOD) from AERONET and synergistic aerosol profiles obtained by combining AERONET sun–sky photometer and ceilometer measurements through the $\text{GRASP}_{\text{pac}}$ algorithm as reference. The two retrieval techniques considered for the ceilometer retrievals are the traditional Klett–Fernald backward inversion and a forward iterative method including an independent calibration procedure. Observations collected at three European stations (Granada, Spain; Payerne, Switzerland; and Lindenberg, Germany) during 2019–2020 are analyzed to assess the performance of both approaches under a wide range of aerosol conditions. The results show that the forward iterative method systematically outperforms the Klett–Fernald backward approach. Under high aerosol load conditions, particularly during coarse-mode-dominated events, the forward retrieval reduces AOD uncertainties by ~ 50 % and achieves root-mean-square errors comparable to those reported in previous validation studies. Vertical comparisons against $\text{GRASP}_{\text{pac}}$ profiles indicate that the forward method maintains consistent accuracy throughout the troposphere, whereas the backward approach exhibits altitude-dependent biases, especially within dust layers. Additional evaluations using COBALD balloon-borne backscatter measurements confirm that the forward retrieval reproduces observed aerosol structures within 10-30 % deviation. These results demonstrate the significant performance gains

https://doi.org/10.5194/egusphere-2026-990
Preprint. Discussion started: 5 March 2026

achieved by operational ceilometer networks when applying forward retrievals with independent calibration under favorable atmospheric conditions.

1 Introduction

Atmospheric aerosols play a crucial role in the Earth's climate system through two main mechanisms: Aerosol–Radiation Interactions (ARI) and Aerosol–Cloud Interactions (ACI) (Forster et al., 2021). ARI involve the direct scattering and absorption of solar radiation, while ACI influence cloud microphysical and optical properties, as aerosols can act as cloud condensation nuclei (CCN) or ice-nucleating particles (INPs), thereby modifying cloud lifetime, albedo, and precipitation processes. The combined Effective Radiative Forcing (ERF) from these processes results in a net cooling of approximately $-1.3\ \mathrm{W\,m^{-2}} \pm 0.7\ \mathrm{W\,m^{-2}}$, with ACI contributing about 75–80 % of the total forcing (Forster et al., 2021). Nevertheless, this forcing exhibits strong regional and temporal variability, largely driven by aerosol composition, atmospheric state, and vertical distribution, which remains one of the least constrained factors (Bellouin et al., 2020).

The pronounced spatial and temporal heterogeneity of aerosols, together with the diversity of their optical, chemical, and physical properties and their complex interactions, makes aerosols one of the largest sources of uncertainty in current climate assessments (Bellouin et al., 2020). Beyond climate, aerosols significantly impact air quality by increasing fine particulate matter ($PM_{2.5}$) concentrations, degrading visibility, and exacerbating respiratory and cardiovascular diseases (Pai et al., 2022). These combined climatic and societal impacts highlight the need for accurate and systematic characterization of aerosol properties across diverse environments and atmospheric conditions. In particular, the vertical distribution of aerosols plays a key role in determining both radiative effects and surface air quality, motivating the use of remote-sensing techniques capable of providing vertically resolved observations.

Ground-based remote sensing offers a unique opportunity to monitor aerosol properties continuously and over large spatial scales. The Aerosol Robotic Network (AERONET; Holben et al., 1998) provides high-quality column-integrated aerosol information using sun–sky photometers, retrieving aerosol optical depth (AOD) and microphysical properties through established inversion algorithms (Dubovik and King, 2000; Dubovik et al., 2006; Sinyuk et al., 2022). However, columnar products alone cannot resolve the vertical structure of aerosol layers, which is essential for understanding aerosol–cloud interactions, long-range transport, and boundary-layer processes.

Vertically resolved aerosol information is obtained from lidar (Light Detection and Ranging) systems, which measure atmospheric backscatter profiles at one or multiple wavelengths. Advanced multi-wavelength Raman lidars allow the independent retrieval of aerosol extinction and backscatter coefficients (Ansmann et al., 1990; Whiteman et al., 1992), and, when combined with elastic channels, enable microphysical inversions (Müller et al., 1999; Böckmann, 2001; Veselovskii et al., 2002). These systems are deployed within networks such as the European Aerosol Research Lidar Network (EARLINET; Wandinger et al., 2016), a core component of the Aerosols, Clouds and Trace Gases

https://doi.org/10.5194/egusphere-2026-990
Preprint. Discussion started: 5 March 2026

Research Infrastructure (ACTRIS; Pappalardo et al., 2014), which has enabled detailed characterization of a wide range of aerosol types.

Despite their scientific value, multi-wavelength Raman lidars face significant operational limitations related to their high cost, system complexity, limited availability, and constraints associated with nighttime operation. Their effective range and vertical resolution depend critically on the signal-to-noise ratio (SNR), which is influenced by both instrumental design and atmospheric conditions (Whiteman et al., 2006, 2011). To overcome these limitations, synergistic retrieval approaches have been developed that combine the vertical profiling capability of elastic lidars with the column-integrated and microphysical information provided by sun–sky photometers.

Representative examples of such synergistic methods include LIRIC (Chaikovsky et al., 2016) and GARRLiC (Lopatin et al., 2013). Building upon these developments, the Generalized Retrieval of Aerosol and Surface Properties (GRASP) algorithm constitutes a flexible and unifying framework rooted in the AERONET inversion heritage (Dubovik et al., 2014, 2021). GRASP enables the retrieval of aerosol properties from diverse combinations of passive and active observations.

A major step for active remote sensing was the integration of the GARRLiC scheme within the GRASP architecture, allowing the synergistic inversion of sun–sky photometer measurements and lidar range-corrected signals. While initially applied to advanced multi-wavelength lidars, the modular design of GRASP enables its extension to simpler systems. The $\text{GRASP}_{\text{pac}}$ configuration (Román et al., 2018) adapts this synergistic concept to single-wavelength ceilometers, combining spectral photometer information with the continuous vertical profiling capability of operational ceilometer networks.

Although multi-wavelength lidars combined with photometers provide highly accurate aerosol retrievals, their cost and operational demands hinder large-scale implementation. In contrast, ceilometers are cost-effective, robust, and designed for unattended long-term operation. Modern ceilometers can detect aerosol layers up to approximately 10 km altitude and are widely deployed within operational networks such as the EUMETNET Ceilometer Network (E-Profile), the Iberian Ceilometer Network (ICENET), and the Italian Automated Ceilometer Network (ALICENET). Their integration with sun–sky photometers through $\text{GRASP}_{\text{pac}}$ further enhances their potential for quantitative aerosol profiling.

Within this framework, the present study evaluates and compares backward and forward ceilometer inversion approaches, both as standalone retrievals and in synergistic combination with sun–sky photometer observations using the GRASP algorithm. In addition, a comprehensive validation strategy focused on the lower troposphere is introduced, employing independent in situ vertical measurements from COBALD balloon-borne sondes to rigorously assess retrieval accuracy and quantify associated uncertainties.

The paper is structured as follows: Sect. 2 describes the instrumentation and datasets, including the ceilometer network and collocated AERONET observations; Sect. 3 outlines the processing chain and retrieval methodologies, including both standalone ceilometer retrievals and the synergistic GRASP approach; Sect. 4 presents the retrieval performance analysis and discusses the main findings; and Sect. 5 summarizes the key conclusions.

https://doi.org/10.5194/egusphere-2026-990
Preprint. Discussion started: 5 March 2026

2 Instrumentation, data and experimental sites

This section provides an overview of the instrumentation and datasets used in this study. Sect. 2.1 describes the three experimental sites, Sect. 2.2 details the remote-sensing instruments and measurement techniques, and Sect. 2.3 presents the in situ observations.

2.1 Stations and datasets

This study was conducted at three European observatories forming a trans-European transect that spans Mediterranean urban, alpine rural, and continental lowland environments. Despite minor temporal data gaps, the complementary datasets collected during the 2019–2020 period enable a robust intercomparison of aerosol properties across contrasting climatic conditions and pollution regimes.

The first site, the Andalusian Global Observatory of the Atmosphere (AGORA), operated by the University of Granada (UGR), is located in the city of Granada, Spain (37.17°N, 3.61°W; 680 m a.s.l.). It represents an urban, non-industrialised environment situated within a mountain basin dominated by the Sierra Nevada range, which rises to nearly 3500 m a.s.l. The station is frequently affected by Saharan dust intrusions (Navas-Guzmán et al., 2013; Pérez-Ramírez et al., 2012; Mandija et al., 2016), local anthropogenic pollution (Titos et al., 2012, 2014), and complex boundary-layer dynamics (Granados-Muñoz et al., 2012; Ortiz-Amezcua et al., 2022).

The second site, the MeteoSwiss Aerological Observatory (PAY), is located in Payerne, Switzerland (46.82°N, 6.95°E; 491 m a.s.l.). It serves as a rural reference station on the Swiss Plateau and is characterised by generally clean air conditions, minimal industrial influence, and frequent winter fog episodes (Navas-Guzmán et al., 2019).

The third site, the Meteorological Observatory Lindenberg (LIN), operated by the Deutscher Wetterdienst (DWD; German Meteorological Service), is located in Lindenberg, Germany (52.21°N, 14.12°E; 120 m a.s.l.). LIN is a supersite dedicated to aerology, radiosounding, remote sensing, radiation measurements, and boundary-layer research, representing a rural lowland environment.

2.2 Remote-sensing instruments

The E-Profile network, a programme of EUMETNET Composite Observing System, provides standardized ceilometer and wind profiler measurements across Europe in near real-time. This network comprises more than 400 stations equipped with various Automatic Lidars and Ceilometers (ALC), providing high-resolution, near-real-time vertical profiles of aerosols, cloud layers, and boundary layer dynamics. E-Profile ensures data homogeneity through calibration procedures and harmonized processing algorithms across instruments and locations, and it provides Level 2 (L2) quality-assured products in the CEDA (Centre for Environmental Data Analysis) database (https://catalogue.ceda.ac.uk).

For this research, data from CHM15k Nimbus ceilometer (Lufft, 2019) was employed. This system is a single-wavelength elastic-backscatter lidar featuring a Nd:YAG (neodymium-doped yttrium–aluminium–garnet) laser that

https://doi.org/10.5194/egusphere-2026-990
Preprint. Discussion started: 5 March 2026

emits 1 ns pulses at 1064 nm. Operating at a 5–7 kHz repetition rate with 8.4 μJ pulse energy and < 0.3 mrad beam divergence, the system detects backscatter signals via an avalanche photodiode (APD) operating in photon-counting mode with a receiver FOV (Field of View) of 0.45 mrad (Martucci et al., 2010).

Column-integrated aerosol optical properties from AERONET (Holben et al., 1998) were used to complement the ceilometer observations. AERONET is a global, ground-based network initiated by NASA and expanded through international collaborations. It employs standardized Cimel sun–sky photometers to provide long-term, high-precision aerosol optical measurements. With over 580 active stations worldwide in diverse environments (urban, rural, coastal, and high-altitude), AERONET provides a comprehensive and publicly accessible dataset essential for climate and air-quality research.

In this study, Cimel Electronique CE318-T sun–sky photometers (Barreto et al., 2016) were used to measure direct solar irradiance and sky radiance at multiple wavelengths covering the 340-1640 nm range. These measurements enable the retrieval of key aerosol properties, including aerosol optical depth, particle size distribution, single-scattering albedo, and complex refractive index. AERONET data are processed in three levels: Level 1.0 (no cloud-screened), Level 1.5 (cloud-screened), and Level 2.0 (quality-assured). To ensure high accuracy and reliability, only version 3 (Giles et al., 2019) level 2.0 data, subject to rigorous calibration and cloud filtering, were employed in this study.

2.3 In situ observations

The Compact Optical Backscatter Aerosol Detector (COBALD) is a lightweight (∼500 g) balloon-borne sonde designed for high-resolution in situ measurements of aerosol and cloud backscatter in the troposphere and lower stratosphere (Brunamonti et al., 2018). Developed at the Swiss Federal Institute of Technology (ETH Zürich) and based on the original prototype by Rosen et al. (1991), COBALD employs two light-emitting diodes (LEDs) at 455 nm and 940 nm, coupled with a photodiode detector featuring a 6° field of view. Originally developed for high-altitude cloud studies (e.g., cirrus and polar stratospheric clouds; (Cirisan et al., 2014)), COBALD has also been proven highly effective for characterizing tropospheric aerosols (Brunamonti et al., 2018, 2021).

The launches were performed at night to minimize solar background noise and prevent detector saturation. Soundings were conducted between 22:00 and 23:00 UTC, with the balloon ascending at approximately 5 ms^{-1}. With a 1 Hz sampling rate, the system achieved a vertical resolution of about 5 m, profiling from the surface up to roughly 30 km, where balloon burst generally occurred.

3 Methodology

This section describes the methodological framework adopted in this study. Section 3.1 presents the calibration procedures and inversion algorithms applied to ceilometer observations. Section 3.2 describes the methodology used to evaluate ceilometer-derived backscatter profiles against independent in situ measurements from COBALD sondes.

https://doi.org/10.5194/egusphere-2026-990
Preprint. Discussion started: 5 March 2026

Section 3.3 outlines the synergistic retrieval approach combining ceilometer and sun–sky photometer observations using the GRASP$_{\mathrm{pac}}$ algorithm. Finally, Section 3.4 details the procedure used to compare ceilometer-derived aerosol optical depth (AOD) with AERONET observations.

3.1 Calibration and inversion algorithms for ceilometer observations

3.1.1 Ceilometer calibration

Accurate calibration is essential for the quantitative retrieval of the aerosol backscatter coefficient $\beta_a(z)$ from ceilometer measurements. The calibration strategy depends on instrument sensitivity, the availability of reference data, and the prevailing atmospheric conditions.

For the CHM15k instruments in E-Profile, calibration is performed using the Rayleigh method (Wiegner and Geiß, 2012; Wiegner et al., 2014). This approach requires the identification of a high-altitude reference region, z_{ref}, typically located in the upper troposphere, where the aerosol backscatter contribution is assumed to be negligible ($\beta_a(z_{\mathrm{ref}}) \approx 0$). Under this assumption, the total atmospheric backscatter at this altitude is attributed exclusively to molecular scattering, such that $\beta(z_{\mathrm{ref}}) = \beta_m(z_{\mathrm{ref}})$. The molecular backscatter coefficient $\beta_m(z_{\mathrm{ref}})$ is calculated using Rayleigh scattering theory together with atmospheric pressure and temperature profiles obtained from numerical models.

The lidar equation can be reformulated in terms of the attenuated backscatter coefficient, β^* (Eq. 1). In this formulation, $P(z)$ denotes the received signal as a function of atmospheric optical properties and measurement range z, while C_{L} represents the system-dependent calibration constant accounting for instrumental characteristics.

$$\frac{P(z)\cdot z^2}{C_L} = \beta^*(z)\cdot \exp\left\{-2\int_0^z \alpha(z')\mathrm{d}z'\right\} \tag{1}$$

The total backscatter coefficient β and the extinction coefficient α are expressed as the sum of aerosol and molecular contributions, i.e., $\beta = \beta_a + \beta_m$ and $\alpha = \alpha_a + \alpha_m$.

The calibration constant C_{L} is obtained by applying the backward Klett–Fernald solution using the reference altitude z_{ref} as boundary condition. Following Wiegner and Geiß (2012); Wiegner et al. (2014), the aerosol backscatter coefficient is computed as

$$\beta_a(z) = \frac{Z(z)}{N(z)} - \beta_m(z), \tag{2}$$

$$Z(z) = z^2 P(z) \exp\left\{-2\int_0^z [S_a(z') - S_m]\beta_m(z')\,\mathrm{d}z'\right\}. \tag{3}$$

https://doi.org/10.5194/egusphere-2026-990
Preprint. Discussion started: 5 March 2026

In this formulation, the aerosol lidar ratio $S_a(z)$ is fixed at 52 sr for calibration within E-Profile, while $S_m \approx 8\pi/3$ sr and $\beta_m(z)$ denote the molecular lidar ratio and molecular backscatter coefficient, respectively.

The auxiliary function $N(z)$ can be formulated in two equivalent ways depending on the adopted boundary condition. It can be expressed explicitly using the system constant C_{L}, which is convenient for forward range integration starting at the lidar, or alternatively in terms of a prescribed reference aerosol backscatter value $\beta_a(z_{\mathrm{ref}})$, which leads to the standard backward integration from the reference altitude toward the instrument. In the E-Profile implementation, $N(z)$ is expressed as

$$N(z) = \frac{z_{\mathrm{ref}}^2\, P(z_{\mathrm{ref}})}{\beta_{\mathrm{m}}(z_{\mathrm{ref}}) + \beta_{\mathrm{a}}(z_{\mathrm{ref}})} + 2 \int_{z}^{z_{\mathrm{ref}}} S_p(z')\, Z(z')\, \mathrm{d}z', \tag{4}$$

where $\beta_a(z_{\mathrm{ref}}) \approx 0$ is assumed for Rayleigh calibration.

A major limitation of Rayleigh calibration arises from the low signal-to-noise ratio (SNR) in the upper troposphere, where ceilometer signals are significantly weaker (Wiegner et al., 2014). Therefore, rigorous filtering of clouds and residual aerosol layers is required to ensure the reliability of the selected calibration interval and to guarantee sufficiently high SNR conditions.

In operational practice, E-Profile applies a calibration procedure that combines long-term signal averaging with careful screening of the reference altitude to minimize the influence of residual aerosols and measurement noise. This procedure requires at least three hours of cloud-free signal integration during nighttime under favourable atmospheric conditions. The resulting calibration constants are subsequently processed using a Kalman filter to derive a daily best estimate of the lidar constant C_{L}, thereby improving the long-term stability and consistency of operational aerosol profiling. A detailed description of the numerical implementation is provided by Wiegner and Geiß (2012); Wiegner et al. (2014).

3.1.2 Forward iterative retrieval

The forward iterative method (Li et al., 2021) solves the lidar equation by integrating upward from the surface, which eliminates the need for a high-altitude, aerosol-free reference and is therefore especially effective under cloudy or low SNR conditions where other methods are unreliable. However, the forward method requires a known system lidar constant C_L as input. This constant is typically obtained from a calibration performed under ideal atmospheric conditions such as clear-sky and high SNR. This approach therefore assumes that the lidar system remains stable between the nighttime calibration and its application during the day.

The algorithm initializes the aerosol backscatter coefficient $\beta_a(z_0)$ at the lowest reliable measurement height, assuming that aerosol transmittance near the surface is approximately unity at infrared wavelengths, so that the initial aerosol backscatter is taken directly from the measured attenuated backscatter (Eq. 5).

https://doi.org/10.5194/egusphere-2026-990
Preprint. Discussion started: 5 March 2026

$$\beta_a(z_0) = \frac{P(z_0) z_0^2}{C_L T_m^2(z_0)} - \beta_m(z_0). \tag{5}$$

From this surface value, the algorithm integrates upward with steps δz. For every new layer $z_i = z_{i-1} + \delta z$, the extinction coefficient is first estimated with the constant lidar ratio S_a of 50 sr in Eq. 6.

$$\alpha_a(z_i) = S_a \, \beta_a(z_{i-1}), \tag{6}$$

Hence, the extinction contributed by that layer is computed in Eq. 7

$$\tau_a(z_i) = \alpha_a(z_i) \, \delta z, \tag{7}$$

and the two-way aerosol transmittance from the surface up to z_i is calculated with Eq. 8

$$T_a(z_i) = \exp\big(-2 \, \tau_a(z_i)\big). \tag{8}$$

With this updated transmittance, the backscatter coefficient at the current level is recomputed from the total attenuated signal with Eq. 9:

$$\beta_a(z_i) = \frac{P(z_i) \, z_i^2}{C_L \, T_m^2(z_i) \, T_a^2(z_i)} - \beta_m(z_i). \tag{9}$$

This process is repeated until the relative change in $\alpha_a(z_i)$ falls below 0.01 % or 30 iterations are reached; the algorithm then steps to the next height and repeats the sequence up to the chosen top of the profile z_{top}.

This approach is particularly robust in aerosol-rich environments, where the backward method often fails due to the absence of a well-defined, aerosol-free reference region aloft. According to Li et al. (2021), a 10 % uncertainty in the system constant C_L leads to a 10–20% error in retrieved β_a within the planetary boundary layer (PBL), while a similar uncertainty in the lidar ratio S_a contributes less than 5 % error. These findings highlight the method's stability in complex aerosol scenes, provided that accurate calibration of C_L is achieved, since errors propagate upward from the surface.

3.1.3 Klett backward retrieval

The analytical backward solution for retrieving the aerosol backscatter coefficient $\beta_a(z)$ from ceilometer measurements, as implemented in the E-Profile framework, is described by Wiegner et al. (2014). In contrast to the forward retrieval approach, the backward method does not require prior knowledge of the system lidar constant C_{L}. Instead, C_{L} is implicitly determined through the application of a boundary condition at a reference altitude where the aerosol contribution is assumed negligible. The explicit value of C_{L} becomes necessary only when switching to a forward integration scheme.

https://doi.org/10.5194/egusphere-2026-990
Preprint. Discussion started: 5 March 2026

A reference altitude z_{ref} is selected in the upper troposphere, where $\beta_a(z_{\mathrm{ref}}) = 0$ is assumed. The molecular backscatter coefficient $\beta_m(z)$ is derived from atmospheric model profiles. The retrieval formulation follows the same mathematical framework used during calibration and is based on Eqs. 1 and 2.

The auxiliary function $Z(z)$ is constructed from the range-corrected signal together with a transmission correction that accounts for differential extinction between aerosol and molecular scattering (Eq. 3). The function $N(z)$ is defined according to Eq. 4.

Under the Rayleigh calibration assumption $\beta_a(z_{\mathrm{ref}}) = 0$, the first term of Eq. 4 simplifies to $z_{\mathrm{ref}}^2 P(z_{\mathrm{ref}})/\beta_m(z_{\mathrm{ref}})$. This term provides the calibration reference by scaling the measured signal at z_{ref} to the known molecular backscatter. The backward solution is then obtained by integrating downward from the reference altitude z_{ref} toward the instrument. The aerosol backscatter coefficient profile is finally retrieved by combining $Z(z)$ and $N(z)$ and subtracting the molecular contribution, as expressed in Eq. 2.

In operational applications, the backward retrieval is subject to several constraints. First, the relatively low optical power of ceilometers requires long signal integration periods to achieve an adequate signal-to-noise ratio (SNR) at the reference altitude z_{ref}, a condition most easily satisfied during nighttime due to reduced background noise. Second, the accuracy of the retrieved $\beta_a(z)$ strongly depends on the assumed aerosol lidar ratio S_a. Although advanced inversion schemes allow S_a to vary with altitude, a constant value of 50 sr is commonly adopted in operational ceilometer processing to convert backscatter coefficients into extinction profiles. Uncertainties in S_a or in the selection of z_{ref} can lead to nonlinear error propagation, particularly under multilayered or vertically inhomogeneous aerosol conditions (Li et al., 2021). Despite these limitations, the backward approach provides a stable and self-calibrating retrieval of $\beta_a(z)$, as it does not require an externally determined lidar constant C_{L}.

3.2 Evaluation of ceilometer backscatter profiles with COBALD in situ measurements

Validation of aerosol backscatter coefficient profiles derived from the CHM15k ceilometer was performed using collocated measurements from Compact Optical Backscatter Aerosol Detector (COBALD) sondes, providing an independent in situ benchmark to assess retrieval accuracy (Brunamonti et al., 2021).

COBALD sondes measure the backscatter ratio (BSR) (Brunamonti et al., 2021), defined as:

$$\beta_{\mathrm{ratio}}(\lambda) = \frac{\beta_{\mathrm{total}}(\lambda)}{\beta_{\mathrm{m}}(\lambda)}, \tag{10}$$

where λ denotes the wavelength (455 or 940 nm), β_{total} is the total backscatter coefficient, and β_{m} is the molecular backscatter coefficient computed from atmospheric extinction (Brunamonti et al., 2021). A BSR value of unity corresponds to purely molecular scattering, while larger values indicate the presence of aerosols or clouds.

For quantitative comparison with ground-based lidar observations, the aerosol backscatter coefficient $\beta_a(z)$ was derived from β_{ratio} assuming a molecular extinction-to-backscatter ratio of $8\pi/3$ sr (Brunamonti et al., 2021). COBALD sondes provide high-resolution β_a profiles at 455 and 940 nm with a vertical resolution of approximately 5 m and a temporal resolution of 1 s during balloon ascent.

https://doi.org/10.5194/egusphere-2026-990
Preprint. Discussion started: 5 March 2026

Since the CHM15k ceilometer operates at 1064 nm, a spectral harmonization step was required to enable a consistent comparison with the COBALD observations at 940 nm. To this end, the aerosol backscatter coefficients retrieved from the ceilometer were spectrally converted from 1064 to 940 nm using an Ångström exponent derived from the dual-wavelength COBALD measurements. The spectral dependence of the aerosol backscatter coefficient was assumed to follow a power-law relationship of the form

$$\beta_a(\lambda_2, z) = \beta_a(\lambda_1, z) \left(\frac{\lambda_2}{\lambda_1} \right)^{-\mathrm{AE}(z)}, \tag{11}$$

where λ_1 and λ_2 represent the ceilometer (1064 nm) and COBALD (940 nm) wavelengths, respectively, and AE(z) is the altitude-dependent Ångström exponent calculated from the ratio of COBALD backscatter coefficients at 455 and 940 nm.

The use of altitude-resolved Ångström exponents allows the spectral conversion to account for vertical variability in aerosol microphysical properties. This approach assumes that the spectral behaviour between 940 and 1064 nm follows the same power-law dependence as between the COBALD measurement wavelengths. Although this assumption introduces additional uncertainty, it provides a reasonable approximation in the near-infrared spectral region under typical tropospheric aerosol conditions.

Following the spectral conversion, COBALD profiles were resampled onto a 15 m vertical grid to match the CHM15k resolution and ensure consistency between datasets. Temporal collocation was achieved by averaging ceilometer backscatter profiles over a 30-minute window corresponding to the COBALD ascent period.

The comparison analysis was restricted to altitudes between 0.25 and 5 km above ground level. Heights below 0.25 km were excluded to avoid the incomplete-overlap region of the ceilometer, while altitudes above 5 km were excluded due to the reduced signal-to-noise ratio of the ceilometer measurements. COBALD launches were performed during nighttime conditions to minimize solar background noise, with soundings typically conducted between 22:00 and 23:00 UTC.

3.3 Ceilometer and sun–sky photometer synergistic approach using GRASP

The modular structure of the Generalized Retrieval of Aerosol and Surface Properties (GRASP) algorithm accommodates a wide range of remote-sensing platforms, including ground-based, airborne, and satellite observations. GRASP comprises two core components: (i) a comprehensive forward radiative transfer model that simulates light interactions with atmospheric constituents, accounting for aerosols, surface reflectance, and molecular scattering, and (ii) an inversion module that applies multi-term least-squares optimization with physical constraints to retrieve multiple atmospheric parameters simultaneously, even under data-limited conditions (Dubovik et al., 2011).

In the GRASP$_{\mathrm{pac}}$ (Photometer And Ceilometer) configuration, AERONET sun–sky photometer measurements are synergistically combined with 1064 nm ceilometer backscatter profiles to retrieve vertically resolved aerosol properties. A key advantage of this approach is that backscatter and extinction coefficients are derived consistently

https://doi.org/10.5194/egusphere-2026-990
Preprint. Discussion started: 5 March 2026

within the inversion framework, with the lidar ratio estimated dynamically rather than prescribed a priori. The retrieval assumes vertically homogeneous intensive aerosol properties, including complex refractive index and single-scattering albedo.

Validation studies have demonstrated strong agreement between $\text{GRASP}_{\text{pac}}$ retrievals and independent in situ measurements, with correlation coefficients exceeding 0.90 for retrieved aerosol volume concentrations (Román et al., 2018). The size distribution is represented using 22 logarithmically spaced bins spanning 0.05–15 μm, and the vertical domain is discretised into 60 logarithmic altitude layers between 250 and 7000 m. Surface reflectance effects are accounted for using MODIS-derived bidirectional reflectance distribution functions (Román et al., 2018).

In this study, AODs processed by the CAELIS system (González et al., 2020) were combined with cloud-screened, Level 2 ceilometer profiles averaged over 30-minute intervals to enhance the signal-to-noise ratio. This synergistic approach is particularly valuable for operational networks lacking advanced multi-wavelength research lidars. $\text{GRASP}_{\text{pac}}$ retrievals used in this work were generated automatically in near real time by the CAECENET system (Herrero del Barrio et al., 2024).

3.4 Comparison of ceilometer-derived AOD with AERONET observations

To further evaluate the performance of the backward and forward ceilometer retrievals, the vertically resolved aerosol backscatter profiles were converted into column-integrated aerosol optical depth (AOD) and compared with independent reference measurements from AERONET sun–sky photometers. This comparison provides an additional validation of the retrieval algorithms by assessing their ability to reproduce the total aerosol optical load within the atmospheric column.

Aerosol backscatter coefficient profiles were retrieved using both backward and forward inversion methods (Sect. 3.1). A cloud-filtering procedure was applied to exclude profiles affected by low-level clouds; specifically, profiles with a detected cloud base below 5 km were removed to avoid integration artefacts. Following cloud screening, extinction profiles were averaged over 30-minute intervals to reduce noise. Aerosol optical depth (AOD) was then obtained by vertically integrating the extinction coefficient from the surface up to 5 km using the trapezoidal rule. This upper integration limit was selected to focus on the lower troposphere, where the majority of atmospheric aerosol mass is typically concentrated (Amiridis et al., 2005).

Ceilometer extinction profiles were derived from Level 2 attenuated backscatter products provided by the E-Profile network, using a fixed lidar ratio of 50 sr for the retrievals similar to previous work (Brunamonti et al., 2021). The processing was performed with the A-Profiles package https://github.com/AugustinMortier/a-profiles. The resulting ceilometer-derived AOD values were subsequently compared against Level 2.0 AERONET observations.

Since AERONET does not provide AOD measurements at 1064 nm (Barreto et al., 2016), the 1020 nm channel was extrapolated to 1064 nm using the Ångström power law. sun–sky photometer AODs were averaged over 30-minute intervals to match the temporal resolution of the ceilometer observations. The agreement between ceilometer-derived

https://doi.org/10.5194/egusphere-2026-990
Preprint. Discussion started: 5 March 2026

AOD (AOD_{Ceil}) and sun–sky photometer AOD (AOD_{SP}) was evaluated using the mean bias, standard deviation (STD), and root-mean-square error (RMSE).

To investigate the dependence of retrieval performance on aerosol loading conditions, the dataset was classified into low and high aerosol load regimes based on daily mean AERONET AOD at 440 nm for the 2019–2020 period. A threshold value of $AOD_{440} = 0.2$ was adopted, with days below this value classified as low load and days equal to or exceeding this threshold classified as high load.

High-load conditions were further categorised according to the AE as a proxy for dominant particle size. Days with AE ≥ 1.2 were classified as fine-mode dominated, typically associated with anthropogenic or biomass-burning aerosols (Reid et al., 2005), whereas days with AE ≤ 0.8 were classified as coarse-mode dominated, generally linked to mineral dust. Days with intermediate AE values ($0.8 < AE < 1.2$) were excluded from this classification, as they represent mixed aerosol conditions without a clearly dominant particle mode.

4 Results and discussion

This section evaluates the performance of the backward and forward ceilometer retrieval methods under a range of atmospheric conditions. The analysis combines independent in situ observations, synergistic retrieval products, and column-integrated aerosol measurements to provide a comprehensive assessment of the retrieval accuracy. First, ceilometer backscatter profiles are validated against collocated COBALD sonde measurements (Sect. 4.1). Second, retrieved backscatter and extinction profiles are compared with synergistic $GRASP_{pac}$ products (Sect. 4.2). Finally, column-integrated aerosol optical depth (AOD) derived from ceilometer observations is evaluated against AERONET measurements (Sect. 4.3). Together, these analyses characterise the performance of both retrieval approaches across different aerosol loading conditions and particle types.

4.1 Evaluation of ceilometer backscatter retrievals using in situ balloon measurements

To assess the accuracy of the ceilometer backscatter retrievals under real atmospheric conditions, aerosol backscatter profiles derived from the CHM15k ceilometer were evaluated against high-resolution in situ measurements from COBALD balloon soundings. The methodological details of the COBALD data processing, spectral harmonization, and spatio-temporal collocation with the ceilometer observations are described in Sect. 3.2.

The comparison focuses on the lower troposphere, between 0.25 and 5 km above ground level (a.g.l.). Heights below 0.25 km were excluded to avoid the incomplete-overlap region of the CHM15k ceilometer (Hervo et al., 2016), while altitudes above 5 km were not considered due to the reduced signal-to-noise ratio of the ceilometer measurements at higher altitudes (Brunamonti et al., 2021). The analysis is based on selected nighttime COBALD soundings, providing independent benchmarks to quantify retrieval uncertainties and to identify potential systematic biases in the lidar-derived aerosol backscatter coefficients in the absence of coincident $GRASP_{pac}$ products.

https://doi.org/10.5194/egusphere-2026-990
Preprint. Discussion started: 5 March 2026

Two representative case studies are examined to illustrate retrieval performance under contrasting aerosol regimes: a Saharan dust event at Payerne and a complex multi-layered case at Lindenberg.

The first case corresponds to a significant Saharan dust intrusion observed at Payerne on 25 June 2019 (Fig. 1). Surface sun–sky photometer measurements reported elevated aerosol optical depths of approximately 0.3–0.4 at 440 nm, together with consistently low AE values (<0.6; Fig. 1a), indicating the dominance of coarse-mode particles. Backward air-mass trajectory analysis using the HYSPLIT model traced the aerosol origin to the Sahara Desert approximately six days prior to the observation. The temporal evolution of the ceilometer-derived backscatter coefficient profiles (Fig. 1b) reveals the continuous presence of dust from 00:00 UTC, with variable layer heights throughout the day and the development of a well-mixed dust layer extending up to about 4 km by nighttime.

The vertical aerosol structure is further characterised in Fig. 2a, which compares backward (orange) and forward (blue) retrievals with coincident COBALD (red) sonde measurements at 23:00 UTC. In this case, the analysis starts at 0.4 km because COBALD sonde measurements below this altitude were not available. Fig. 2a shows backscatter coefficient profiles at 940 nm, from layer top height ∼4 km upward all three profiles tend to a molecular zone where both backward and forward methods shows noise contamination. All three profiles exhibit consistent dust layer structure from 0.4 to 3.5 km; however, the forward retrieval achieves closer agreement with the COBALD reference measurements. The corresponding AE profile obtained from COBALD shows a decrease from 0.8 at 1.5 km to 0.4 at 4 km (Fig. 2b), consistent with the sun–sky photometer–derived values and confirming coarse-mode dominance throughout the column. Fig. 2c and d shows the deviations and relative deviations between the backward and forward retrievals against COBALD, indicating that the forward profile agrees well with COBALD throughout the dust layer with smaller deviations.

Table 1 presents a quantitative comparison between the two retrieval methods and the COBALD sonde data. From the lowest altitude up to 4 km, backward retrieval shows an underestimation with respect to COBALD while forward retrieval shows a slight overestimation until 1.8 km height, from this altitude upwards it shows underestimation. The backward method yields systematically large negative backscatter coefficients (-0.22 to -0.35 $\mathrm{Mm^{-1}\ sr^{-1}}$) and greater relative deviations (-23 to -34 %) than the forward method (0.88 to -0.020 $\mathrm{Mm^{-1}\ sr^{-1}}$, 10 to -17 %). This discrepancy peaks in the 3–4 km layer, where dust loading was maximal (backward: -0.35 $\mathrm{Mm^{-1}\ sr^{-1}}$; forward: -0.20 $\mathrm{Mm^{-1}\ sr^{-1}}$). Above the dust layer (4–5 km), both methods converge to similar values but with significant noise due to lack of power of ceilometer laser, although the backward method maintains a slightly smaller relative deviation (-20 % vs. -53 %).

These differences indicate that, while both methods successfully capture the dust plume's vertical structure, the backward method's sensitivity to contamination of the reference layer under dense aerosol conditions produces larger deviations. The forward method shows superior agreement with sonde measurements (Table 1), maintaining low deviations relative to COBALD throughout the tropospheric column. This case represents a well-documented episode of long-range Saharan dust transport, exhibiting notable temporal persistence (>24 hours) and vertical extent (0–4 km). The consistent coarse-mode signature across all instruments suggests minimal particle modification

https://doi.org/10.5194/egusphere-2026-990
Preprint. Discussion started: 5 March 2026

during transport, while the method-dependent differences highlight the importance of algorithm selection for dust monitoring applications.

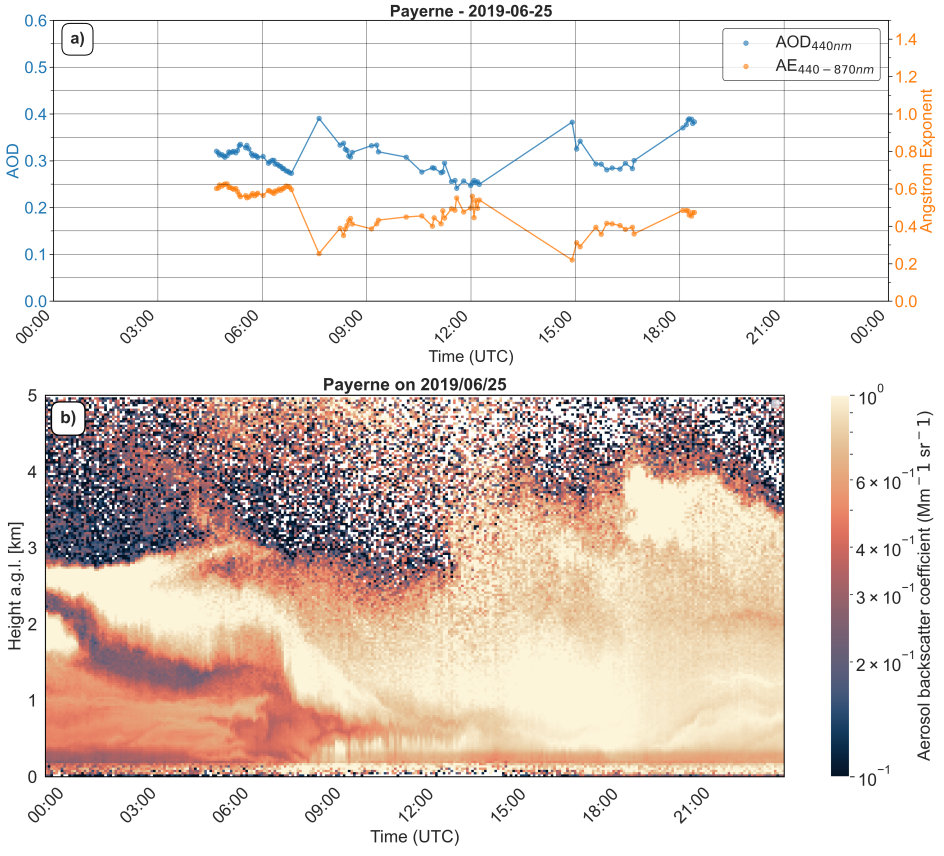

Figure 1. Characterization of the dust outbreak event over Payerne a) AOD (440 nm) and Ångström exponent (440-870 nm); b) ceilometer aerosol backscatter coefficient with forward retrieval

https://doi.org/10.5194/egusphere-2026-990
Preprint. Discussion started: 5 March 2026

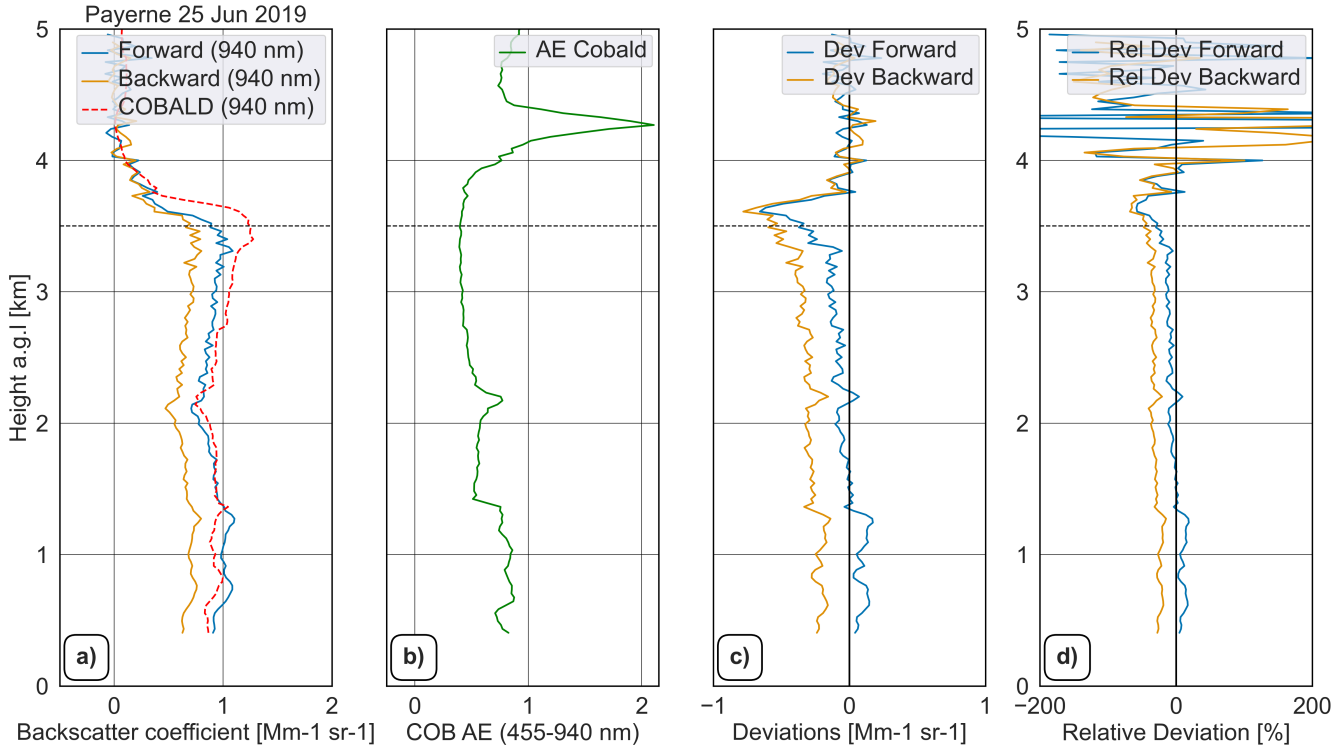

Figure 2. 30 min averaged profile comparison between forward/backward retrievals versus COBALD sonde for 25 June 2019. Panel a shows the backward (yellow) forward (blue) and COBALD (red) profile, next panel (b) shows the Ångström exponent profile of COBALD and the following panels (c and d) show the deviation and relative deviation of Backward-COBALD (yellow) and Forward-COBALD (blue)

Table 1. Mean deviations between ceilometer retrievals (backward and forward) against COBALD measurements showing profile deviation and relative deviation

Height	**Backward deviations**		**Forward deviations**	
km	**$Mm^{-1}sr^{-1}$**	**%**	**$Mm^{-1}sr^{-1}$**	**%**
0.4-1	-0.22	-23	0.88	10
1-2	-0.25	-27	0.02	3
2-3	-0.30	-32	-0.08	-8
3-4	-0.35	-34	-0.20	-17
4-5	-0.03	-20	-0.03	-53

The second case, observed on 27 August 2020 at Lindenberg, exemplifies the challenges faced by ceilometer aerosol retrievals under highly unfavourable atmospheric conditions. Persistent rainfall until 15:00 UTC precluded the availability of reliable AERONET observations, and the subsequent clearing phase was characterised by the presence

https://doi.org/10.5194/egusphere-2026-990
Preprint. Discussion started: 5 March 2026

of a residual cloud layer at approximately 2 km altitude (Fig. 3). Above this level, ceilometer signals were largely dominated by noise, resulting in particularly demanding conditions for the retrieval algorithms. A comparison with COBALD sonde measurements acquired at 22:00 UTC (Fig. 4a) reveals marked differences between the two inversion approaches. The forward method shows very good agreement with the in situ observations, yielding small negative deviations in the lowest layer (0.25–1 km: -0.03 Mm^{-1} sr^{-1}) and within the 1–2 km a.g.l. layer (0.01 Mm^{-1} sr^{-1}), corresponding to moderate relative deviations of -8 % and 8 %, respectively. In contrast, the backward method performs poorly below 2 km, producing large and physically unrealistic deviations associated with an overestimation of the aerosol backscatter coefficient (1.98–2.00 Mm^{-1} sr^{-1}) and extreme relative deviations ranging from 337 % to 2020 %. Owing to the negligible signal-to-noise ratio above 2 km, the quantitative analysis is restricted to the lower troposphere.

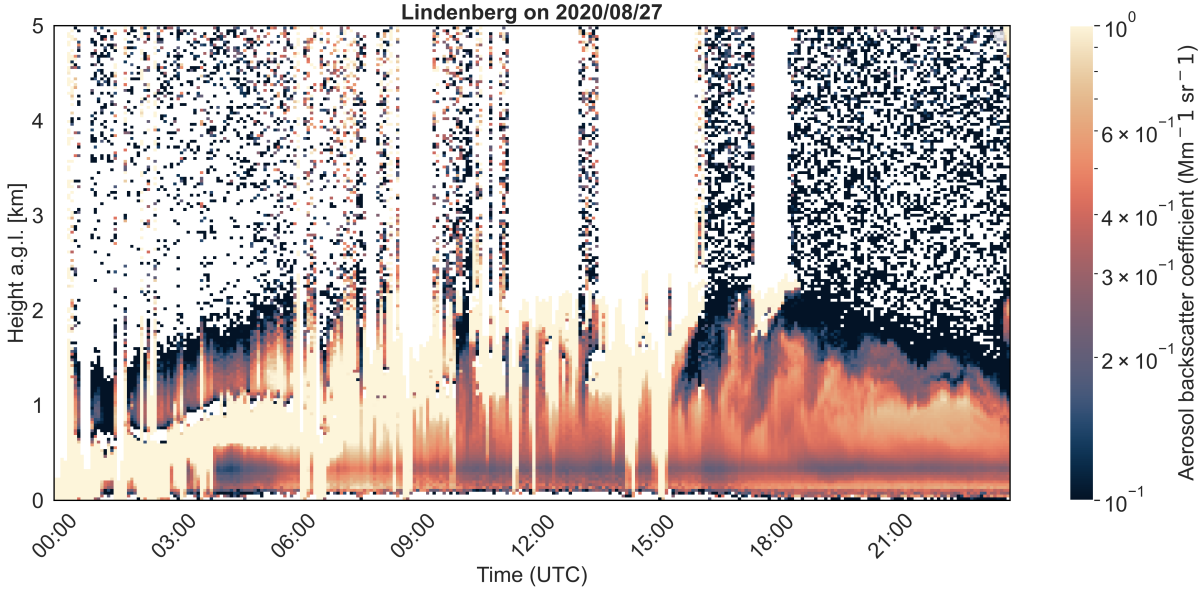

Figure 3. Temporal evolution of forward retrieval aerosol backscatter coefficient from the ceilometer for the day 27 August 2020

The degraded performance of the backward retrieval is attributed to the absence of a reliable, aerosol-free reference altitude. Above ∼2 km, SNR drops, causing the Klett-Fernald integration to retrieve on noise rather than molecular scattering, which propagates an unrealistic backscatter profile downward.

The AE profile (Fig. 4b) reveals vertically stratified aerosol properties: coarse-mode dominance (AE <0.8) below 1.2 km, mixed aerosol types (AE ∼1.0) between 1.2–2 km, and almost no particle presence at higher altitudes (Fig. 3b). Quantitative deviation analysis (Fig. 3c and d) shows how the forward method maintains strong agreement with COBALD within the aerosol layer (-8 to 8 % deviation), while the backward method exhibits severe biases that exceed 300 %. This case study clearly demonstrates the forward method's superior robustness for nighttime

https://doi.org/10.5194/egusphere-2026-990
Preprint. Discussion started: 5 March 2026

aerosol characterization, particularly under complex vertical structures and high noise contamination. The backward method's complete failure in the aerosol layer and poor performance aloft underscore its limitations for operational use under such conditions, contrasting with its better behaviour in the Payerne case where higher altitudes were less affected by noise.

These case studies illustrate the operational advantages of the forward iterative method over the traditional backward retrieval. The forward retrieval and its calibration avoids the need for an aerosol-free reference altitude, resulting in more accurate, vertically consistent profiles with significantly reduced bias when validated against in situ observations.

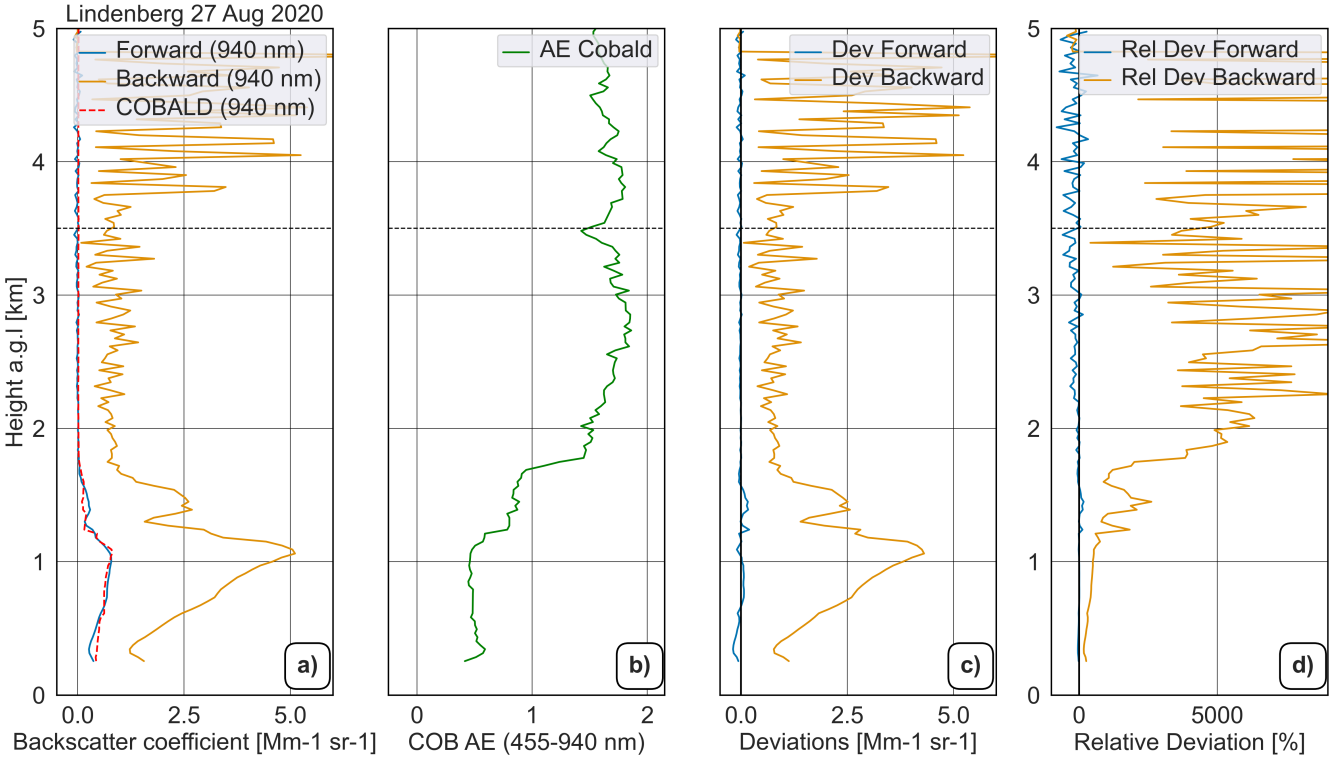

Figure 4. 30 min averaged profile comparison between forward/backward retrievals versus COBALD sonde for 27 August 2020. Panel a show the backward (yellow) forward (blue) and COBALD (red) profile, next panel (b) show the Ångström exponent profile of COBALD and the following panels (c and d) show the deviation and relative deviation of Backward-COBALD (yellow) and Forward-COBALD (blue)

4.2 Extinction and backscatter comparison against GRASPpac retrievals

Following the validation with COBALD, the evaluation is extended by comparing ceilometer-derived backscatter and extinction profiles with synergistic retrievals from $\text{GRASP}_{\text{pac}}$. $\text{GRASP}_{\text{pac}}$ combines sun–sky photometer and

https://doi.org/10.5194/egusphere-2026-990
Preprint. Discussion started: 5 March 2026

ceilometer data without a priori lidar ratio assumptions. This comparison assesses retrieval consistency across diverse aerosol regimes at three European sites: Granada, Payerne, and Lindenberg.

Backscatter and extinction coefficients are analyzed because they offer complementary insights into retrieval performance. The aerosol backscatter coefficient represents the primary information directly contained in the elastic lidar signal and can typically be retrieved with good accuracy under standard conditions (Ansmann and Müller, 2005). While extinction is retrieved and escalated by the assumed lidar ratio. Studying backscatter therefore offers a robust assessment of each algorithm's ability to resolve vertical aerosol structure accurately.

Deviation profiles were computed between ceilometer retrievals and $\mathrm{GRASP_{pac}}$. To minimize the influence of outliers, only data within the 10th–90th percentile range were retained. The mean and standard deviation of the differences were subsequently calculated, following the aerosol scenarios previously mention in Sect. 3.4. For this analysis, profiles were divided into two layers: a lower layer from 0.25–2 km and an upper layer from 2–5 km. This stratification distinguishes near-surface regions—which are typically more influenced by aerosol presence from higher altitudes where aerosol concentrations are generally lower.

4.2.1 Backscatter coefficient assessment against $\mathbf{GRASP_{pac}}$

To evaluate the performance of the backward and forward methods in retrieving aerosol vertical structure, backscatter coefficient profiles are compared from both approaches against the synergistic $\mathrm{GRASP_{pac}}$ algorithm. The evaluation spans different aerosol regimes at the three European stations: Granada, Payerne, and Lindenberg (Fig. 5).

Although both retrieval methods generally agree with the $\mathrm{GRASP_{pac}}$ reference in a general scenario, significant biases emerge under high aerosol load, particularly during coarse-mode events that are frequent at the Granada site (Table 2). The forward method consistently outperforms the backward approach, reducing near surface bias by approximately a factor of three under coarse particle conditions. This demonstrates the forward retrieval's robustness in environments where clean-air reference altitudes are unavailable or contaminated.

At Granada, considering the full dataset, the backward retrieval shows a systematic positive bias of 0.027 ± 0.194 $\mathrm{Mm^{-1}sr^{-1}}$ within the 0.25–2 km layer, whereas the forward retrieval shifts the mean to -0.028 ± 0.079 $\mathrm{Mm^{-1}sr^{-1}}$, reducing the spread by more than half (Table 2). Between 2–5 km, the backward results exhibit a slightly negative deviation with greater scatter (-0.005 ± 0.109 $\mathrm{Mm^{-1}sr^{-1}}$), while the forward retrieval maintains a negative mean with relative dispersion below 35 %. The increasing negative deviation with height reflects the systematic error propagation characteristic of backward integration when the boundary value at the molecular reference altitude is poorly constrained (Klett, 1981). In contrast, the forward method removes this altitude-dependent trend and maintains uniform agreement throughout the troposphere (Fig. 5a).

Under high aerosol optical depth (AOD) conditions, the sign of the deviation reverses: the backward retrieval shows deviations of -0.454 ± 0.304 $\mathrm{Mm^{-1}sr^{-1}}$ (0.25-2 km) and -0.420 ± 0.310 $\mathrm{Mm^{-1}sr^{-1}}$ (2-5 km), while the forward retrieval reduces both to -0.168 ± 0.167 and -0.161 ± 0.169 $\mathrm{Mm^{-1}sr^{-1}}$ respectively. The big deviations in the backward method comparison reflects its vulnerability to error propagation due to inability of finding a free aerosol

https://doi.org/10.5194/egusphere-2026-990
Preprint. Discussion started: 5 March 2026

region. The forward approach avoids this effect, maintaining an altitude-independent bias and demonstrating superior performance under dust-rich and low-signal conditions (Fig. 5b).

For cases dominated by coarse-mode particles, the backward bias peaks at -0.551 ± 0.262 $Mm^{-1}sr^{-1}$ near the surface and -0.500 ± 0.283 $Mm^{-1}sr^{-1}$ at higher altitudes. The forward method again reduces the bias by approximately a factor of three (-0.200 ± 0.158 and -0.191 ± 0.165 $Mm^{-1}sr^{-1}$) and maintains relative dispersion below 30 % at all heights (Table 2). This results indicate that the forward method correctly retrieves the strong scattering from large particles in contrast to backward method.

Under fine-mode-dominated conditions, both algorithms underestimate the backscatter coefficient, though in different ways. For the 0.25–2 km layer, the backward method yields -0.123 ± 0.271 $Mm^{-1}sr^{-1}$ and -0.032 ± 0.125 $Mm^{-1}sr^{-1}$ for the upper range, while the forward retrieval reduces both the mean deviation and dispersion by approximately ~ 50 % (-0.054 ± 0.163 and -0.020 ± 0.069 $Mm^{-1}sr^{-1}$). The largest relative deviation occurs in the boundary layer, where fine aerosols are concentrated, and decreases with height. The forward method preserves this physically consistent gradient while tightening the spread, indicating a better representation of fine-particle vertical structure. It is also important to note that differences in the prescribed lidar ratio between the forward/backward retrievals and the dynamically adjusted lidar ratio in $GRASP_{pac}$ may partly explain the discrepancies observed under high aerosol load for both fine- and coarse-mode-dominated cases.

At Payerne, the altitude-dependent behaviour is similar to that observed at Granada. The comparison of the full dataset shows a nearly constant negative backward bias with height (-0.129 ± 0.167 and -0.077 ± 0.116 $Mm^{-1}sr^{-1}$ for the 0.5-2 km and 2-5 km layers, respectively), while the forward retrieval centres the mean deviation profile near zero and reduces the dispersion 10 % with respect to backward for the 0.5-2 km layer (Fig. 5i). During high-aerosol-load episodes, the deviations remain negative, but the forward method keeps a deviation of -0.012 $Mm^{-1}sr^{-1}$ and reduces the relative deviation by approximately 40 % while backward shows deviations greater than -0.170 $Mm^{-1}sr^{-1}$ (Fig. 5j). Coarse-mode conditions amplify the vertical gradient with backward ($-0.481 \pm 0.229, -0.383 \pm 0.229$ $Mm^{-1}sr^{-1}$; Table 2), yet the forward retrieval reduces the mean deviation to -0.092 $Mm^{-1}sr^{-1}$ and -0.106 $Mm^{-1}sr^{-1}$ (Fig. 5k). Fine-mode pollution introduces a stronger negative deviation in the 0.5–2 km layer (-0.207 ± 0.211 $Mm^{-1}sr^{-1}$) with backward that weakens with height; forward retrievals again exhibit narrower dispersion across all layers. Overall, Payerne reproduces the vertical patterns observed at Granada, confirming that the retrieval algorithm remains robust despite site-specific microphysical differences.

Lindenberg shows a behaviour broadly comparable to Granada, although with weaker systematic trends and a stronger influence of case-to-case variability. For the full dataset, both retrievals exhibit small negative biases, with the forward method yielding values closer to zero and a reduced dispersion compared to the backward approach (Fig. 5i) . In contrast to Granada, no pronounced altitude-dependent increase of the backward bias is observed at this site. Under high aerosol load conditions, deviations remain moderate for both retrievals, while the forward method consistently reduces the spread of the differences, indicating improved stability (23 % versus 44 %) in the 0.25-2 km layer. Coarse-mode-dominated cases exhibit larger negative biases, particularly for the backward

https://doi.org/10.5194/egusphere-2026-990
Preprint. Discussion started: 5 March 2026

retrieval, although these deviations are less pronounced than those observed at Granada. The forward method substantially mitigates these biases, reducing their magnitude by approximately 50-60 % (Table 2); however, this result should be interpreted with caution due to the limited number of available cases (eight events). For fine-mode-dominated conditions, both retrievals tend to underestimate the $GRASP_{pac}$ backscatter coefficient, but the forward approach maintains a noticeably narrower dispersion, particularly in the lower troposphere (relative variability of approximately 23 % compared to about 45 % for the backward method). Overall, the Lindenberg results confirm the improved robustness of the forward retrieval, while highlighting the role of variable air-mass history and more complex aerosol mixtures in shaping site-specific variability.

In summary, the forward method consistently outperforms the traditional backward approach across all aerosol regimes. Key improvements include eliminating the altitude-dependent bias characteristic of the backward kernel, reducing mean deviation significantly, and yielding smaller standard deviations in backscatter coefficient profiles. This enhanced performance is most evident under challenging conditions such as high aerosol load and coarse-mode particle dominance.

https://doi.org/10.5194/egusphere-2026-990
Preprint. Discussion started: 5 March 2026

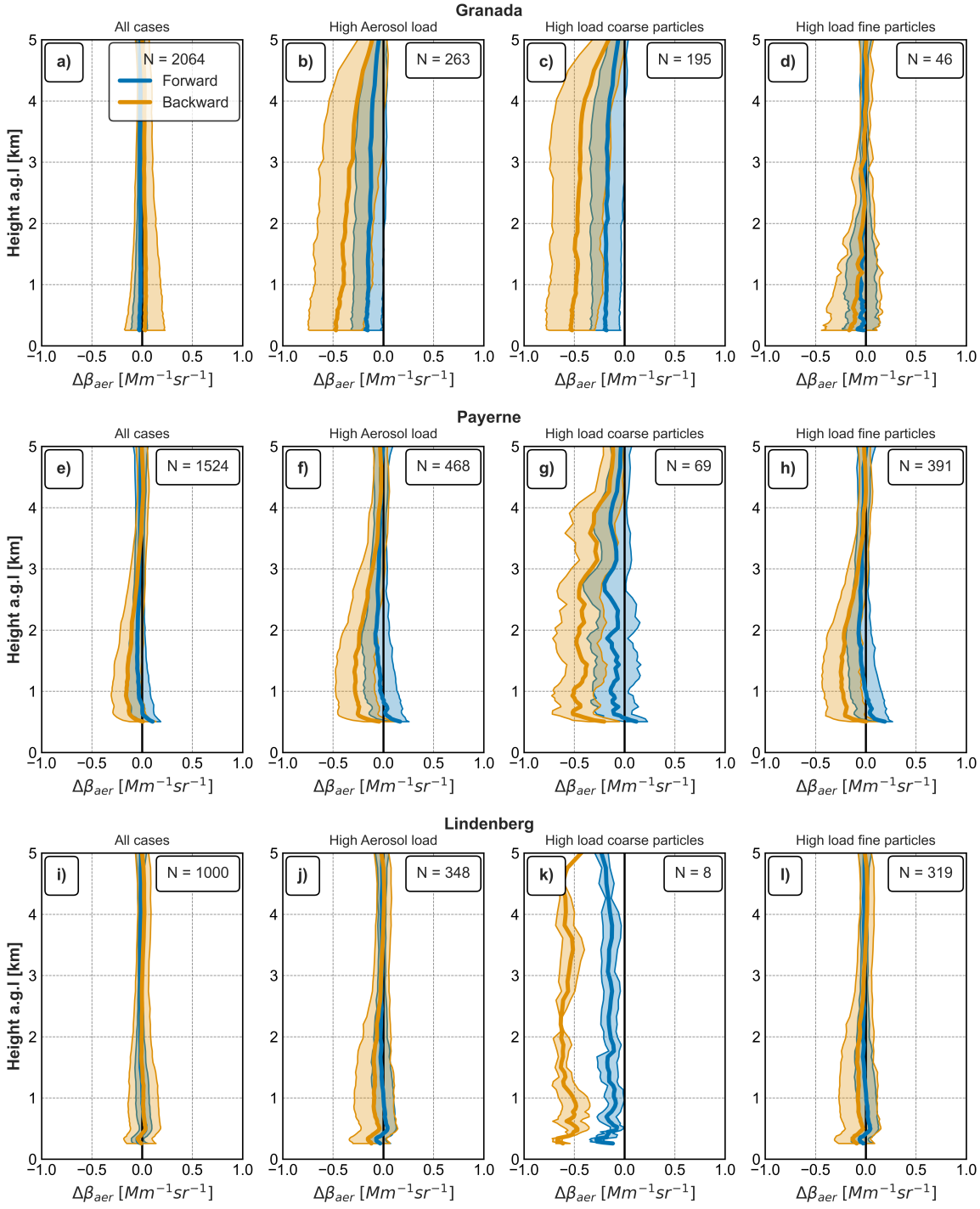

Figure 5. Tropospheric backscatter coefficient profiles comparison: Klett-Fernald backward retrievals versus $\text{GRASP}_{\text{pac}}$ for Granada (top), Payerne (middle) and Lindenberg (bottom) with the full dataset (a, e, i), high aerosol load (b, f, j), coarse dominated particles (c, g, k), fine dominated particles (d, h, l) aerosol conditions and N shows number of profiles in each panel

https://doi.org/10.5194/egusphere-2026-990
Preprint. Discussion started: 5 March 2026

Table 2. Statistical analysis of mean ± standard deviation and relative deviations (%) of backscatter coefficient comparison between backward/forward method against $GRASP_{pac}$ for Granada (UGR), Payerne (PAY) and Lindenberg (LIN) under different aerosol load and particle-mode conditions showing mean ± standard deviation between $GRASP_{pac}$

		Layers	All data				High aerosol load				High aerosol load coarse particles				High aerosol load fine particles			
			$Mm^{-1}sr^{-1}$		%		$Mm^{-1}sr^{-1}$		%		$Mm^{-1}sr^{-1}$		%		$Mm^{-1}sr^{-1}$		%	
		km	Mean	STD	Mean	STD	Mean	STD	Mean	STD	Mean	STD	Mean	STD	Mean	STD	Mean	STD
UGR	Backward	2-5	−0.005	0.109	−32	123	−0.420	0.310	−66	26	−0.500	0.283	−73	19	−0.032	0.125	−7	63
		0.25-2	0.027	0.194	25	83	−0.454	0.304	−54	26	−0.551	0.262	−63	19	−0.123	0.271	−9	45
	Forward	2-5	−0.027	0.049	−36	34	−0.161	0.169	−25	19	−0.191	0.165	−26	17	−0.020	0.069	−16	35
		0.25-2	−0.028	0.079	−9	27	−0.168	0.167	−20	18	−0.200	0.158	−24	16	−0.054	0.163	−4	28
PAY	Backward	2-5	−0.077	0.116	−37	91	−0.172	0.166	−62	42	−0.383	0.229	−73	18	−0.129	0.143	−56	54
		0.5-2	−0.129	0.167	−34	53	−0.251	0.216	−44	34	−0.481	0.229	−64	15	−0.207	0.211	−39	38
	Forward	2-5	−0.041	0.074	−40	63	−0.060	0.112	−29	44	−0.106	0.184	−18	31	−0.054	0.096	−33	49
		0.5-2	−0.019	0.111	−2	42	−0.012	0.164	4	35	−0.092	0.215	−7	28	0.003	0.154	6	35
LIN	Backward	2-5	−0.012	0.089	−15	108	−0.052	0.120	−20	59	−0.578	0.120	−92	3	−0.042	0.111	−11	64
		0.25-2	0.003	0.160	9	64	−0.096	0.204	−14	44	−0.564	0.106	−93	5	−0.083	0.199	−12	45
	Forward	2-5	−0.020	0.040	−34	43	−0.023	0.064	−15	33	−0.191	0.080	−29	10	−0.021	0.058	−17	34
		0.25-2	−0.007	0.070	−1	27	−0.018	0.103	−1	23	−0.157	0.089	−27	13	−0.013	0.098	−1	23

4.2.2 Comparison of extinction profiles retrieved by backward and forward methods using $GRASP_{pac}$

Aerosol extinction profiles retrieved from ceilometer observations using the backward (Klett-Fernald) and forward (iterative) approaches are evaluated against the synergistic $GRASP_{pac}$ products, which combine sun–sky photometer and ceilometer measurements and provide vertically resolved extinction without prescribing a fixed lidar ratio (Sect. 3.3). The comparison is performed for three European sites and for different aerosol regimes (Fig. 6, Table 3).

Across all stations and conditions, the forward retrieval systematically reduces the dispersion of extinction differences relative to $GRASP_{pac}$, while the backward method exhibits stronger altitude-dependent biases. For the complete dataset, relative variability is typically reduced by 30-60% when using the forward approach, with the magnitude of the improvement depending on aerosol load and dominant particle size.

At Granada, the backward method shows pronounced biases throughout the tropospheric column, with mean deviations of 6.6 ± 9.2 Mm^{-1} below 2 km and 1.6 ± 4.4 Mm^{-1} between 2 and 5 km. The forward retrieval reduces these values to 3.2 ± 4.0 Mm^{-1} and 0.2 ± 2.0 Mm^{-1}, respectively. Under high aerosol load and coarse-mode-dominated conditions, the backward approach strongly underestimates extinction, whereas the forward method reduces the magnitude of these deviations by up to 60-70 %, particularly above the boundary layer. For fine-mode dominance,

https://doi.org/10.5194/egusphere-2026-990
Preprint. Discussion started: 5 March 2026

both retrievals overestimate extinction near the surface, but the forward approach reduces the relative dispersion by about ~ 50 %.

At Payerne, deviations are generally smaller but exhibit a stronger dependence on aerosol regime. For the complete dataset, the backward retrieval underestimates extinction in both altitude ranges (-2.6 ± 7.1 Mm^{-1} below 2 km), while the forward method yields comparable mean positive deviations with reduced variability. Under high aerosol load, the backward method maintains a negative bias near the surface, whereas the forward retrieval shifts the mean deviation towards positive values and reduces the dispersion, particularly between 2 and 5 km. Coarse-mode-dominated cases again highlight the limitations of the backward approach, with negative deviations reduced by a factor of three to four when using the forward method.

At Lindenberg, extinction differences display weaker systematic trends but larger case-to-case variability. For the full dataset, the backward method exhibits a positive bias below 2 km (3.9 ± 7.5 Mm^{-1}) that decreases with height, while the forward retrieval reduces both the mean bias and the dispersion. Under high aerosol load, the forward approach does not consistently improve the mean bias but reduces the relative variability by roughly a factor of two. Coarse-mode-dominated events produce the largest discrepancies, with strong underestimation by the backward method throughout the column (-23.9 ± 3.9 Mm^{-1} below 2 km), which is substantially mitigated by the forward retrieval. This result should, however, be interpreted with caution due to the limited number of coarse-mode cases at this site. Under fine-mode dominance, both retrievals overestimate extinction in the lower troposphere, but the forward approach maintains a markedly narrower dispersion at all altitudes.

Comparison against GRASP$_{\mathrm{pac}}$ reveals smaller dispersion for backscatter than extinction coefficients (Tables 2 and 3). This difference can be attributed from the distinct sensitivity to the lidar ratio (S_a). Backscatter is retrieved directly from the measured signal with a weaker sensitivity, whereas extinction is computed as $\alpha(z) = S_a \cdot \beta(z)$, inheriting both backscatter uncertainty and the full uncertainty in the assumed lidar ratio. Since GRASP$_{\mathrm{pac}}$ retrieves S_a dynamically, extinction deviations reflect the mismatch between assumed and actual aerosol-specific lidar ratios, explaining the larger dispersion.

Overall, the comparison with GRASP$_{\mathrm{pac}}$ demonstrates that the forward iterative retrieval provides a more stable and vertically consistent representation of aerosol extinction than the traditional backward approach. The improvement is most pronounced under high aerosol load and coarse-mode-dominated conditions, supporting the suitability of the forward method for operational aerosol profiling with ceilometer networks.

https://doi.org/10.5194/egusphere-2026-990
Preprint. Discussion started: 5 March 2026

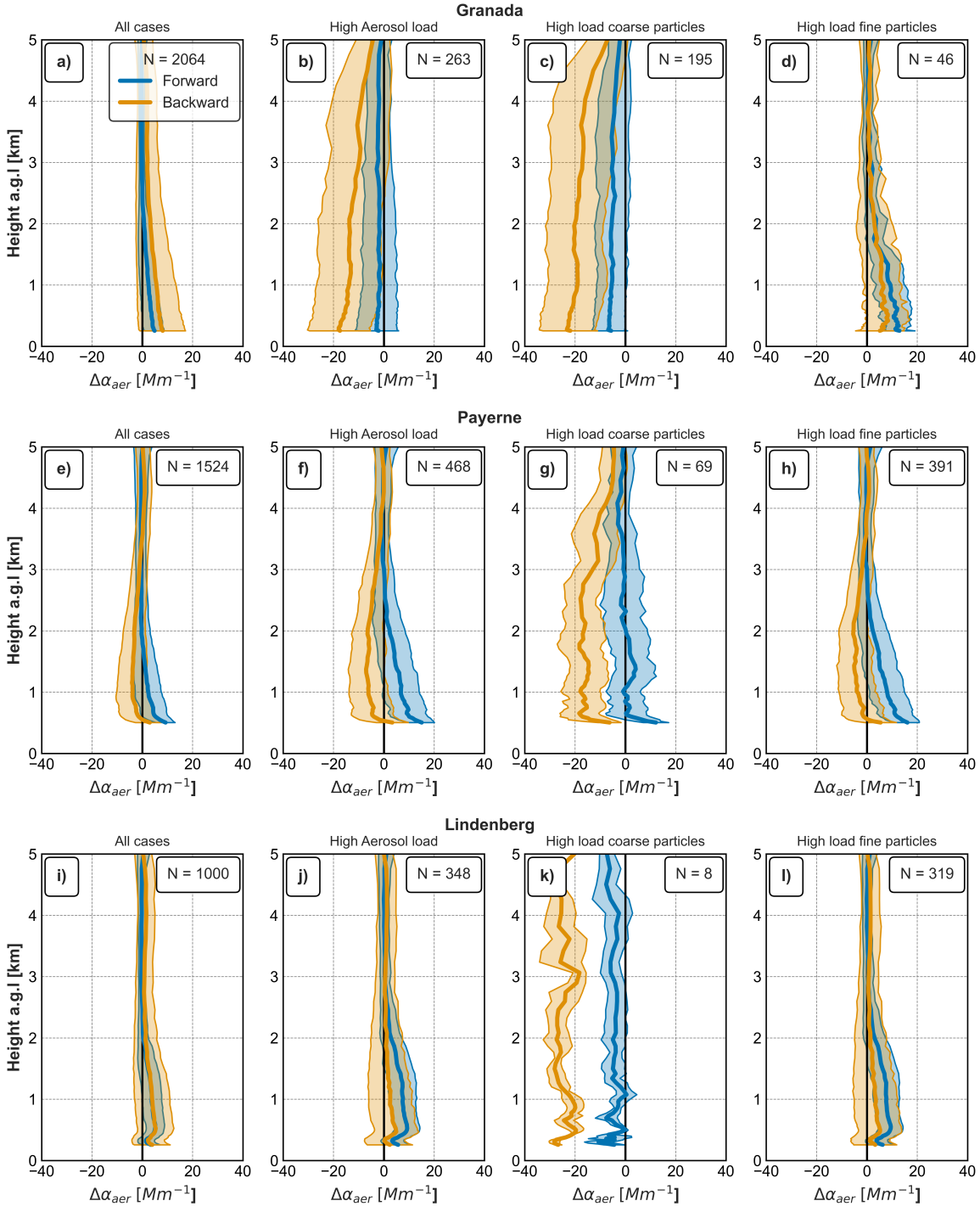

Figure 6. Tropospheric extinction profiles comparison: differences between Klett-Fernald backward retrieval - $GRASP_{pac}$ for Granada (top), Payerne (middle) and Lindenberg (bottom) with the full dataset (a, e, i), high aerosol load (b, f, j), coarse dominated particles (c, g, k), fine dominated particles (d, h, l) aerosol conditions and N shows the number of profiles in each panel.

https://doi.org/10.5194/egusphere-2026-990
Preprint. Discussion started: 5 March 2026

Table 3. Statistical analysis of mean ± standard deviation and relative deviations (%) of extinction comparison between backward/forward method against $GRASP_{pac}$ for Granada (UGR), Payerne (PAY) and Lindenberg (LIN) under different aerosol load and particle-mode conditions.

		Layers	All data				High aerosol load				High aerosol load coarse particles				High aerosol load fine particles			
			Mm^{-1}		%		Mm^{-1}		%		Mm^{-1}		%		Mm^{-1}		%	
		km	Mean	STD	Mean	STD	Mean	STD	Mean	STD	Mean	STD	Mean	STD	Mean	STD	Mean	STD
UGR	Backward	2-5	1.6	4.4	80	163	−14.8	13.2	−58	34	−20.5	12.5	−70	22	2.1	5.2	44	86
		0.25-2	6.6	9.2	71	109	−15.7	13.7	−43	34	−22.6	11.8	−58	22	6.3	9.4	38	61
	Forward	2-5	0.2	2.0	12	47	−3.4	6.6	−14	24	−6.0	6.7	−20	18	2.0	3.6	29	52
		0.25-2	3.2	4.0	22	38	−2.2	8.1	−6	24	−6.0	6.9	−17	18	9.8	6.3	43	26
PAY	Backward	2-5	−2.0	4.3	−20	113	−4.8	6.1	−47	58	−14.1	7.8	−67	20	−3.2	5.1	−37	73
		0.5-2	−2.6	7.0	−17	64	−4.8	8.5	−23	45	−16.9	8.2	−55	18	−2.6	8.3	−14	52
	Forward	2-5	−0.5	3.1	−21	81	0.4	4.8	−1	62	−1.1	6.7	−4	33	0.5	4.2	−2	71
		0.5-2	2.8	5.4	28	53	7.2	7.4	46	49	2.2	7.8	14	29	8.1	7.1	52	51
LIN	Backward	2-5	0.7	3.8	45	131	0.3	4.9	15	84	−25.0	6.5	−91	4	0.7	4.8	26	89
		0.25-2	3.8	7.5	39	79	2.6	9.3	21	64	−23.9	3.9	−92	6	3.4	9.1	26	66
	Forward	2-5	0.1	2.0	−11	57	1.6	3.2	24	49	−6.5	4.7	−21	14	1.5	3.1	23	51
		0.25-2	3.3	4.0	25	35	6.5	5.3	38	33	−4.1	4.0	−19	17	6.8	5.2	40	33

4.3 Comparison of column-integrated extinction using AERONET AOD

The column-level consistency of ceilometer aerosol retrievals is evaluated by vertically integrating extinction profiles derived with the Klett-Fernald backward and forward iterative methods to obtain aerosol optical depth (AOD), which is compared against AERONET Level 2.0 observations (Sect. 3.4). Figure 7 summarizes the AOD deviations for the different aerosol regimes, while the associated statistical metrics are reported in Table 4.

For the complete dataset (first column in each panel of Fig. 7), a good overall agreement is found between ceilometer-derived AOD and AERONET at all three stations. Forward retrievals exhibit mean biases close to zero at UGR, PAY, and LIN, indicating the absence of systematic over- or underestimation. The corresponding standard deviations are approximately ±0.01, comparable to the intrinsic uncertainty of AERONET AOD. In contrast, backward retrievals show larger mean biases and dispersion except for LIN, with standard deviations ranging from ±0.024 at Payerne to ±0.035 at Granada, i.e. roughly three times higher than those of the forward method. This demonstrates the improved stability of the forward approach, which benefits from a calibration performed under favourable atmospheric conditions.

From an uncertainty perspective, the forward retrieval consistently yields lower absolute and relative standard deviations while maintaining a mean bias statistically indistinguishable from zero. According to the *Guide to the*

https://doi.org/10.5194/egusphere-2026-990
Preprint. Discussion started: 5 March 2026

Expression of Uncertainty in Measurement (JCFG/GUM, 2008, 2020), this behaviour indicates negligible systematic uncertainty and confirms the adequacy of the adopted random uncertainty model. It should be noted that these evaluations were restricted to daytime hours, conditions under which the backward method faces additional limitations due to reduced SNR.

Under high aerosol load conditions (second column of Fig. 7), deviations between ceilometer and AERONET AOD increase, particularly at UGR. There, the backward method exhibits the largest discrepancy, with a mean bias of -0.103 and a standard deviation of ± 0.076, whereas the forward retrieval reduces both the bias and dispersion to -0.043 and ± 0.050, respectively. Similar but weaker improvements are observed at PAY (-0.033 versus 0.005) and LIN (-0.018 versus -0.008). In all cases, the relative standard deviation of the forward retrieval remains below 30 %, while that of the backward method exceeds this threshold, reflecting the greater sensitivity of the backward approach to contamination of the reference altitude under high aerosol load.

When filtering by particle mode, the largest AOD deviations are found for coarse-mode-dominated conditions. For the backward method, mean differences range from -0.116 to -0.184 across the three stations, corresponding to relative deviations exceeding -70 %, although with more moderate dispersion ($\sim$20 %). The forward retrieval substantially reduces these mean deviations to values below -55 % at all sites, while the standard deviation remains similar between both approaches (Table 4). For fine-mode-dominated conditions, both methods exhibit smaller mean biases, with deviations generally below 0.020 at all stations, except for the backward retrieval at PAY. Nevertheless, the forward approach consistently shows lower dispersion (about 20 % compared to $\sim$60 % for the backward method at UGR and LIN), highlighting its improved robustness. The remaining discrepancies can be attributed to the use of a fixed lidar ratio of 50 sr, which is not optimal for all aerosol types.

The performance of the forward method is consistent with recent GRASP-MPLNET intercomparisons (Lopatin et al., 2024), which reported RMSE values of 0.022–0.038 at 532 nm. In the present study, forward retrievals yield RMSE values of 0.012 at Granada, 0.010 at Payerne, and 0.013 at Lindenberg, confirming comparable or improved agreement when the same photometric reference is employed.

In summary, the forward iterative method reproduces AOD more accurately and with significantly lower dispersion than the traditional Klett-Fernald backward approach across geographically distinct sites. The improvement is particularly evident under challenging tropospheric conditions, such as high aerosol load and coarse-mode particle dominance, where the backward method is more sensitive to reference-altitude contamination. The enhanced performance of the forward approach can be attributed to its refined calibration strategy, combined with the temporal stability of the ceilometer system, which allows calibration parameters to be reliably transferred over time. The systematic reduction of data dispersion, together with the absence of significant mean bias, supports the operational use of ceilometers coupled with forward retrieval algorithms for AOD monitoring in dust-influenced and polluted environments, and highlights the critical role of high-quality instrument calibration.

https://doi.org/10.5194/egusphere-2026-990
Preprint. Discussion started: 5 March 2026

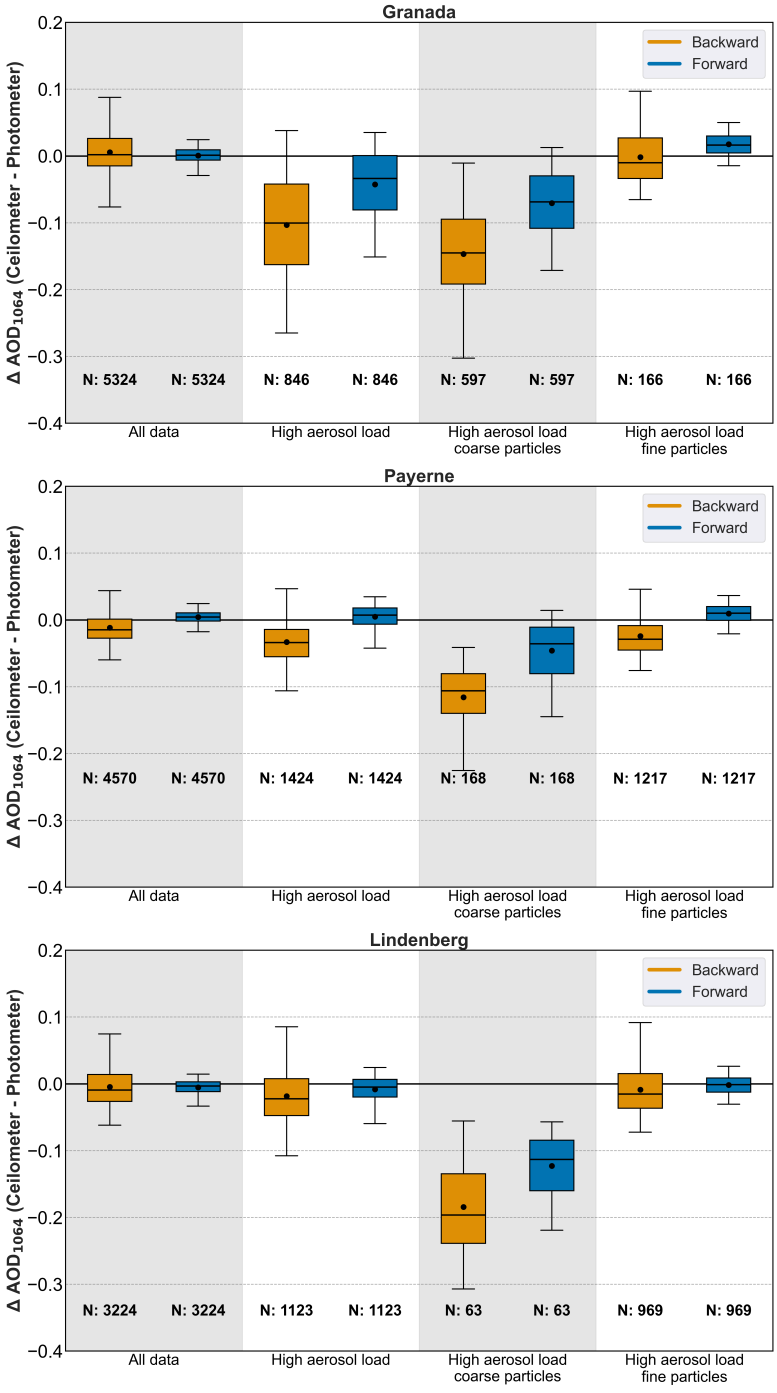

Figure 7. Deviations between Ceilometer AOD retrieved by both backward (yellow) and forward (blue) algorithm against AERONET sun–sky photometer AOD at Granada (upper panel), Payerne (middle panel) and Lindenberg (lower panel). From left to right: all cases, high load, high load coarse particles and high load fine particles. The whiskers of each box show the interquartile range, the dot and black line inside the boxes represent the mean and median respectively and the N shows the number of integrated profiles used.

https://doi.org/10.5194/egusphere-2026-990
Preprint. Discussion started: 5 March 2026

Table 4. Deviation mean, Standard Deviation (STD), relative differences (%) and RMSE to compare ceilometer integrated AOD versus AERONET AOD at Granada (UGR), Payerne (PAY) and Lindenberg (LIN) .

		All data			High aerosol load			High aerosol load coarse particles			High aerosol load fine particles		
		Mean %	STD %	RMSE	Mean %	STD %	RMSE	Mean %	STD %	RMSE	Mean %	STD %	RMSE
UGR	Backward	0.006 35	0.035 95	0.035	-0.103 -56	0.076 35	0.128	-0.147 -71	0.067 22	0.161	0.002 4	0.041 61	0.041
	Forward	0.001 6	0.012 29	0.012	-0.043 -18	0.050 27	0.066	-0.070 -33	0.047 17	0.085	0.018 25	0.017 23	0.024
PAY	Backward	-0.012 -23	0.024 58	0.027	-0.033 -41	0.033 40	0.047	-0.116 -75	0.047 19	0.125	-0.024 -41	0.029 58	0.038
	Forward	0.004 13	0.009 29	0.010	0.005 11	0.018 24	0.018	-0.046 -24	0.042 17	0.062	-0.010 -24	0.014 46	0.017
LIN	Backward	-0.005 -3	0.031 64	0.032	-0.018 -19	0.041 51	0.045	-0.184 -81	0.068 14	0.196	-0.009 -9	0.038 54	0.039
	Forward	-0.005 -8	0.011 20	0.013	-0.008 -7	0.020 22	0.021	-0.123 -53	0.045 10	0.131	-0.002 -1	0.014 20	0.014

5 Conclusions

This study has assessed the capability of operational ceilometers to retrieve aerosol backscatter and extinction profiles through a comprehensive evaluation against independent reference datasets. Ceilometer-based retrievals obtained using both the traditional Klett-Fernald backward inversion and a forward iterative method were compared with synergistic $\text{GRASP}_{\text{pac}}$ products, which combine sun–sky photometer and ceilometer observations, as well as with in situ balloon-borne COBALD measurements. The analysis was conducted at three European sites (Granada, Payerne, and Lindenberg) covering a wide range of aerosol types, loading conditions, and meteorological regimes.

The results demonstrate that the forward iterative retrieval systematically outperforms the conventional backward approach. This improvement is primarily linked to the calibration strategy of the forward method, which relies on a single, independently determined calibration constant combined with the temporal stability of the ceilometer system, rather than on a profile-by-profile calibration based on a reference altitude. It is noted that the $\text{GRASP}_{\text{pac}}$ and AERONET evaluations were conducted during daytime, when the backward method faces additional challenges such as a reduced SNR in contrast to forward only night calibration. Across all sites and aerosol regimes, the forward method consistently reduces the dispersion of retrieved backscatter and extinction profiles and mitigates altitude-dependent biases that are characteristic of the backward inversion.

The benefits of the forward approach are most evident under high aerosol load and coarse-mode-dominated conditions, where the backward method is particularly sensitive to uncertainties in the selection of an aerosol-free reference region and tends to underestimate extinction. In these cases, the forward retrieval substantially reduces the magnitude of the deviations and provides a more vertically coherent representation of aerosol layers. Under fine-mode-dominated conditions, both retrieval approaches may exhibit residual biases, especially within the boundary layer, reflecting the limitations imposed by the use of a fixed lidar ratio; nevertheless, the forward method consistently yields

https://doi.org/10.5194/egusphere-2026-990
Preprint. Discussion started: 5 March 2026

lower variability and improved stability. Validation against high-resolution COBALD soundings further confirms the robustness of the forward retrieval in the lower and middle troposphere.

The comparison with $GRASP_{pac}$ highlights the value of synergistic inversions combining ceilometer and sun–sky photometer data as a reference framework for evaluating ceilometer-based algorithms. A key advantage of $GRASP_{pac}$ is its ability to adjust the lidar ratio dynamically within each retrieval. The close agreement observed between $GRASP_{pac}$ products and the forward ceilometer retrieval indicates that, when properly calibrated, single-wavelength ceilometer inversions can reproduce the main features of more complex multi-instrument solutions.

At the column-integrated level, forward-derived AOD values show good agreement with AERONET observations at all sites, with mean biases close to zero and standard deviations comparable to the intrinsic uncertainty of AERONET AOD. In contrast, backward retrievals exhibit substantially larger dispersion, particularly under high aerosol load and coarse-mode-dominated conditions. These results confirm that the improved vertical consistency of the forward method translates directly into more stable and reliable column-integrated aerosol properties.

From an operational perspective, the findings support the integration of forward iterative ceilometer retrievals into existing observational networks such as E-Profile and ICENET. The combination of low maintenance requirements, continuous operation, and dense spatial coverage makes ceilometers a cost-effective complement to advanced multi-wavelength lidar systems, enhancing regional and continental aerosol monitoring capabilities.

In summary, this study demonstrates that the forward iterative retrieval provides a more robust and vertically consistent representation of aerosol backscatter and extinction than the traditional Klett-Fernald backward inversion. While extinction retrievals remain sensitive to lidar ratio assumptions, backscatter profiles exhibit lower uncertainty and higher reliability. Together, these results establish operational ceilometers, when carefully calibrated and quality-controlled, as practical and sustainable sources of vertically resolved aerosol information, contributing meaningfully to long-term air quality monitoring and climate-related atmospheric research.

Data availability. AERONET data are available at https://aeronet.gsfc.nasa.gov. Ceilometer data from E-Profile are available through CEDA at https://catalogue.ceda.ac.uk/. COBALD data are available upon request

Author contributions. JMR, AC, and FNG conceptualized the study and developed the methodology. JMR, AC, FNG, ES, AH, CHB, RR, PLMM performed the formal analysis and data curation. FNG, AC, and AH provided supervision. JMR wrote the original manuscript draft, which was reviewed and edited by all authors. FNG administered the project and acquired funding.

Competing interests. The authors declare that they have no conflict of interest

https://doi.org/10.5194/egusphere-2026-990
Preprint. Discussion started: 5 March 2026

Acknowledgements

This research was funded by the grants PID2021-128008OB-I00 and PID2024-162154OB-I00, funded by the Spanish Ministry of Science, Innovation and Universities (MICIU/AEI/10.13039/501100011033) and co-funded by the European Regional Development Fund (ERDF/EU). This work is also part of the Spanish national projects CNS2023-145435 and PID2023-151817OA-I00, as well as the Horizon Europe programme under the Marie Skłodowska-Curie Staff Exchange Action project GRASP-SYNERGY (grant agreement No. 101131631). The study made use of the strategic research networks RED2022-134824-E and RED2024-153821-E, and infrastructure grants EQC2019-006192-P and EQC2019-006423-P, funded by MCIN/AEI/10.13039/501100011033. Additional support was provided through the ATMO-ACCESS project (grant agreement No. 101008004), the ACTRIS-IMP project (grant agreement No. 871115), and the Scientific Unit of Excellence: Earth System (UCE-PP2017-02). This work was also partially funded by the AEROMOST project (ProExcel_00204) of the Junta de Andalucía. Francisco Navas-Guzmán acknowledges funding from the Ramón y Cajal programme (ref. RYC2019-027519-I) of the Spanish Ministry of Science and Innovation. Part of this work was supported by COST Action EARLICOST (CA24135), funded by COST (European Cooperation in Science and Technology). Víctor Manuel Naval Hernández acknowledges support from the Spanish Ministry of Science, Innovation and Universities through the FPU grant FPU23/01327, co-funded by the European Social Fund Plus.

List of acronyms

Acronym	Description
ACI	Aerosol-Cloud Interactions
ACTRIS	Aerosols, Clouds and Trace Gas Research Infrastructure
AE	Ångström exponent
AERONET	Aerosol Robotic Network
a.g.l.	Above ground level
AGORA	Andalusian Global Observatory of the Atmosphere
ALC	Automatic Lidars and Ceilometers
AOD	Aerosol Optical Depth
APD	Avalanche Photodiode
ARI	Aerosol-Radiation Interactions
BSR	Backscatter Ratio

Continued on next page

https://doi.org/10.5194/egusphere-2026-990
Preprint. Discussion started: 5 March 2026

Acronym	Description
CCN	Cloud Condensation Nuclei
COBALD	Compact Optical Backscatter Aerosol Detector
DWD	Deutscher Wetterdienst (German Meteorological Service)
EARLINET	European Aerosol Research Lidar Network
E-PROFILE	EUCOS observation programme for measuring profiles of winds, clouds and aerosols
ERF	Effective Radiative Forcing
EUCOS	EUMETNET Composite Observing System
EUMETNET	European Meteorological Network
FOV	Field Of View
GARRLiC	Generalized Aerosol Retrieval from Radiometer and Lidar
GRASP	Generalized Retrieval of Aerosol and Surface Properties
GUM (JCFG)	Guide to the Expression of Uncertainty in Measurement
ICENET	Iberian Ceilometer Network
INP	Ice-Nucleating Particles
LED	Light-Emitting Diode
LIDAR	Light Detection and Ranging
LIN	Abbreviation for Observatory Lindenberg (DWD)
LIRIC	LIdar-Radiometer Inversion Code
MOL-RAO	Meteorological Observatory Lindenberg - Richard-Assmann-Observatory (DWD)
NASA	National Aeronautics and Space Administration
PAY	Abbreviation for Observatory Payerne (MeteoSwiss)
PBL	Planetary Boundary Layer
PM	Particle Matter
RCS	Range-Corrected Signal
RMSE	Root-Mean-Square-Error
SNR	Signal to Noise Ratio
STD	Standard Deviation
UGR	University of Granada

https://doi.org/10.5194/egusphere-2026-990
Preprint. Discussion started: 5 March 2026

References

Amiridis, V., Balis, D. S., Kazadzis, S., Bais, A., Giannakaki, E., Papayannis, A., and Zerefos, C.: Four-year aerosol observations with a Raman lidar at Thessaloniki, Greece, in the framework of European Aerosol Research Lidar Network (EARLINET), Journal of Geophysical Research: Atmospheres, 110, https://doi.org/https://doi.org/10.1029/2005JD006190, 2005.

Ansmann, A. and Müller, D.: Lidar and Atmospheric Aerosol Particles, pp. 105–141, Springer New York, New York, NY, https://doi.org/10.1007/0-387-25101-4_4, 2005.

Ansmann, A., Riebesell, M., and Weitkamp, C.: Measurement of atmospheric aerosol extinction profiles with a Raman lidar, Optics letters, 15, 746–748, 1990.

Barreto, A., Cuevas, E., Granados-Muñoz, M.-J., Alados-Arboledas, L., Romero, P. M., Gröbner, J., Kouremeti, N., Almansa, A. F., Stone, T., Toledano, C., Román, R., Sorokin, M., Holben, B., Canini, M., and Yela, M.: The new sun-sky-lunar Cimel CE318-T multiband photometer – a comprehensive performance evaluation, Atmospheric Measurement Techniques, 9, 631–654, https://doi.org/10.5194/amt-9-631-2016, 2016.

Bellouin, N., Quaas, J., Gryspeerdt, E., Kinne, S., Stier, P., Watson-Parris, D., Boucher, O., Carslaw, K. S., Christensen, M., Daniau, A.-L., Dufresne, J.-L., Feingold, G., Fiedler, S., Forster, P., Gettelman, A., Haywood, J. M., Lohmann, U., Malavelle, F., Mauritsen, T., McCoy, D. T., Myhre, G., Mülmenstädt, J., Neubauer, D., Possner, A., Rugenstein, M., Sato, Y., Schulz, M., Schwartz, S. E., Sourdeval, O., Storelvmo, T., Toll, V., Winker, D., and Stevens, B.: Bounding Global Aerosol Radiative Forcing of Climate Change, Reviews of Geophysics, 58, e2019RG000660, https://doi.org/https://doi.org/10.1029/2019RG000660, e2019RG000660 10.1029/2019RG000660, 2020.

Böckmann, C.: Hybrid regularization method for the ill-posed inversion of multiwavelength lidar data in the retrieval of aerosol size distributions, Applied Optics, 40, 1329–1342, 2001.

Brunamonti, S., Jorge, T., Oelsner, P., Hanumanthu, S., Singh, B. B., Kumar, K. R., Sonbawne, S., Meier, S., Singh, D., Wienhold, F. G., Luo, B. P., Boettcher, M., Poltera, Y., Jauhiainen, H., Kayastha, R., Karmacharya, J., Dirksen, R., Naja, M., Rex, M., Fadnavis, S., and Peter, T.: Balloon-borne measurements of temperature, water vapor, ozone and aerosol backscatter on the southern slopes of the Himalayas during StratoClim 2016–2017, Atmospheric Chemistry and Physics, 18, 15 937–15 957, https://doi.org/10.5194/acp-18-15937-2018, 2018.

Brunamonti, S., Martucci, G., Romanens, G., Poltera, Y., Wienhold, F. G., Hervo, M., Haefele, A., and Navas-Guzmán, F.: Validation of aerosol backscatter profiles from Raman lidar and ceilometer using balloon-borne measurements, Atmospheric Chemistry and Physics, 21, 2267–2285, https://doi.org/10.5194/acp-21-2267-2021, 2021.

Chaikovsky, A., Dubovik, O., Holben, B., Bril, A., Goloub, P., Tanré, D., Pappalardo, G., Wandinger, U., Chaikovskaya, L., Denisov, S., et al.: Lidar-Radiometer Inversion Code (LIRIC) for the retrieval of vertical aerosol properties from combined lidar/radiometer data: development and distribution in EARLINET, Atmospheric Measurement Techniques, 9, 1181–1205, 2016.

Cirisan, A., Luo, B. P., Engel, I., Wienhold, F. G., Sprenger, M., Krieger, U. K., Weers, U., Romanens, G., Levrat, G., Jeannet, P., Ruffieux, D., Philipona, R., Calpini, B., Spichtinger, P., and Peter, T.: Balloon-borne match measurements of

https://doi.org/10.5194/egusphere-2026-990
Preprint. Discussion started: 5 March 2026

midlatitude cirrus clouds, Atmospheric Chemistry and Physics, 14, 7341–7365, https://doi.org/10.5194/acp-14-7341-2014, 2014.

Dubovik, O. and King, M. D.: A flexible inversion algorithm for retrieval of aerosol optical properties from Sun and sky radiance measurements, Journal of Geophysical Research: Atmospheres, 105, 20 673–20 696, https://doi.org/https://doi.org/10.1029/2000JD900282, 2000.

Dubovik, O., Sinyuk, A., Lapyonok, T., Holben, B. N., Mishchenko, M., Yang, P., Eck, T. F., Volten, H., Muñoz, O., Veihelmann, B., et al.: Application of spheroid models to account for aerosol particle nonsphericity in remote sensing of desert dust, Journal of Geophysical Research: Atmospheres, 111, 2006.

Dubovik, O., Herman, M., Holdak, A., Lapyonok, T., Tanré, D., Deuzé, J. L., Ducos, F., Sinyuk, A., and Lopatin, A.: Statistically optimized inversion algorithm for enhanced retrieval of aerosol properties from spectral multi-angle polarimetric satellite observations, Atmospheric Measurement Techniques, 4, 975–1018, https://doi.org/10.5194/amt-4-975-2011, 2011.

Dubovik, O., Lapyonok, T., Litvinov, P., Herman, M., Fuertes, D., Ducos, F., Lopatin, A., Chaikovsky, A., Torres, B., Derimian, Y., et al.: GRASP: a versatile algorithm for characterizing the atmosphere, Spie Newsroom, 25, 2–1201 408, 2014.

Dubovik, O., Fuertes, D., Litvinov, P., Lopatin, A., Lapyonok, T., Doubovik, I., Xu, F., Ducos, F., Chen, C., Torres, B., Derimian, Y., Li, L., Herreras-Giralda, M., Herrera, M., Karol, Y., Matar, C., Schuster, G. L., Espinosa, R., Puthukkudy, A., Li, Z., Fischer, J., Preusker, R., Cuesta, J., Kreuter, A., Cede, A., Aspetsberger, M., Marth, D., Bindreiter, L., Hangler, A., Lanzinger, V., Holter, C., and Federspiel, C.: A Comprehensive Description of Multi-Term LSM for Applying Multiple a Priori Constraints in Problems of Atmospheric Remote Sensing: GRASP Algorithm, Concept, and Applications, Frontiers in Remote Sensing, Volume 2 - 2021, https://doi.org/10.3389/frsen.2021.706851, 2021.

Forster, P., Storelvmo, T., Armour, K., Collins, W., Dufresne, J.-L., Frame, D., Lunt, D., Mauritsen, T., Palmer, M., Watanabe, M., Wild, M., and Zhang, H.: The Earth's Energy Budget, Climate Feedbacks, and Climate Sensitivity, p. 923–1054, Cambridge University Press, Cambridge, United Kingdom and New York, NY, USA, https://doi.org/10.1017/9781009157896.009, 2021.

Giles, D. M., Sinyuk, A., Sorokin, M. G., Schafer, J. S., Smirnov, A., Slutsker, I., Eck, T. F., Holben, B. N., Lewis, J. R., Campbell, J. R., Welton, E. J., Korkin, S. V., and Lyapustin, A. I.: Advancements in the Aerosol Robotic Network (AERONET) Version 3 database – automated near-real-time quality control algorithm with improved cloud screening for Sun photometer aerosol optical depth (AOD) measurements, Atmospheric Measurement Techniques, 12, 169–209, https://doi.org/10.5194/amt-12-169-2019, 2019.

González, R., Toledano, C., Román, R., Fuertes, D., Berjón, A., Mateos, D., Guirado-Fuentes, C., Velasco-Merino, C., Antuña Sánchez, J. C., Calle, A., Cachorro, V. E., and de Frutos, A. M.: Daytime and nighttime aerosol optical depth implementation in CÆLIS, Geoscientific Instrumentation, Methods and Data Systems, 9, 417–433, https://doi.org/10.5194/gi-9-417-2020, 2020.

Granados-Muñoz, M. J., Navas-Guzmán, F., Bravo-Aranda, J. A., Guerrero-Rascado, J. L., Lyamani, H., Fernández-Gálvez, J., and Alados-Arboledas, L.: Automatic determination of the planetary boundary layer height using lidar: One-year analysis over southeastern Spain, Journal of Geophysical Research: Atmospheres, 117, https://doi.org/https://doi.org/10.1029/2012JD017524, 2012.

https://doi.org/10.5194/egusphere-2026-990
Preprint. Discussion started: 5 March 2026

Herrero del Barrio, C., Román, R., González, R., Cazorla, A., Herreras-Giralda, M., Antuña-Sánchez, J. C., Molero, F., Navas-Guzmán, F., Serrano, A., Obregón, M. A., Sola, Y., Pandolfi, M., Herrero-Anta, S., González-Fernández, D., Muñiz-Rosado, J., Mateos, D., Calle, A., Toledano, C., Cachorro, V. E., and de Frutos, A. M.: CAECENET: An automatic system processing photometer and ceilometer data from different networks to provide columnar and vertically-resolved aerosol properties, PLOS ONE, 19, 1–23, https://doi.org/10.1371/journal.pone.0311990, 2024.

Hervo, M., Poltera, Y., and Haefele, A.: An empirical method to correct for temperature-dependent variations in the overlap function of CHM15k ceilometers, Atmospheric Measurement Techniques, 9, 2947–2959, https://doi.org/10.5194/amt-9-2947-2016, 2016.

Holben, B., Eck, T., Slutsker, I., Tanré, D., Buis, J., Setzer, A., Vermote, E., Reagan, J., Kaufman, Y., Nakajima, T., Lavenu, F., Jankowiak, I., and Smirnov, A.: AERONET—A Federated Instrument Network and Data Archive for Aerosol Characterization, Remote Sensing of Environment, 66, 1–16, https://doi.org/https://doi.org/10.1016/S0034-4257(98)00031-5, 1998.

JCFG/GUM: Evaluation of measurement data — Guide to the expression of uncertainty in measurement, https://www.bipm.org/documents/20126/2071204/JCGM_100_2008_E.pdf, jCGM 100:2008, 2008.

JCFG/GUM: Guide to the Expression of Uncertainty in Measurement — Part 6: Developing and Using Measurement Models, https://www.bipm.org/documents/20126/2071204/JCGM_GUM_6_2020.pdf, jCGM GUM 6:2020, 2020.

Klett, J. D.: Stable analytical inversion solution for processing lidar returns, Appl. Opt., 20, 211–220, https://doi.org/10.1364/AO.20.000211, 1981.

Li, D., Wu, Y., Gross, B., and Moshary, F.: Capabilities of an Automatic Lidar Ceilometer to Retrieve Aerosol Characteristics within the Planetary Boundary Layer, Remote Sensing, 13, https://doi.org/10.3390/rs13183626, 2021.

Lopatin, A., Dubovik, O., Chaikovsky, A., Goloub, P., Lapyonok, T., Tanré, D., and Litvinov, P.: Enhancement of aerosol characterization using synergy of lidar and sun-photometer coincident observations: the GARRLiC algorithm, Atmospheric Measurement Techniques, 6, 2065–2088, https://doi.org/10.5194/amt-6-2065-2013, 2013.

Lopatin, A., Dubovik, O., Stenchikov, G., Welton, E. J., Shevchenko, I., Fuertes, D., Herreras-Giralda, M., Lapyonok, T., and Smirnov, A.: Comparison of diurnal aerosol products retrieved from combinations of micro-pulse lidar and sun photometer observations over the KAUST observation site, Atmospheric Measurement Techniques, 17, 4445–4470, 2024.

Lufft: User Manual: Lufft CHM 15K Ceilometer, Lufft GmbH, Fellbach, Germany, https://www.lufft.com/download/manual-chm15k-en/, last accessed: 21 April 2025, 2019.

Mandija, F., Guerrero-Rascado, J. L., Lyamani, H., Granados-Muñoz, M. J., and Alados-Arboledas, L.: Synergic estimation of columnar integrated aerosol properties and their vertical resolved profiles in respect to the scenarios of dust intrusions over Granada, Atmospheric Environment, 145, 439–454, https://doi.org/https://doi.org/10.1016/j.atmosenv.2016.09.045, 2016.

Martucci, G., Milroy, C., and O'Dowd, C. D.: Detection of Cloud-Base Height Using Jenoptik CHM15K and Vaisala CL31 Ceilometers, Journal of Atmospheric and Oceanic Technology, 27, 305 – 318, https://doi.org/10.1175/2009JTECHA1326.1, 2010.

Müller, D., Wandinger, U., and Ansmann, A.: Microphysical particle parameters from extinction and backscatter lidar data by inversion with regularization: theory, Applied Optics, 38, 2346–2357, 1999.

https://doi.org/10.5194/egusphere-2026-990
Preprint. Discussion started: 5 March 2026

Navas-Guzmán, F., Bravo-Aranda, J. A., Guerrero-Rascado, J. L., Granados-Muñoz, M. J., and Alados-Arboledas, L.: Statistical analysis of aerosol optical properties retrieved by Raman lidar over Southeastern Spain, Tellus B: Chemical and Physical Meteorology, https://doi.org/10.3402/tellusb.v65i0.21234, 2013.

Navas-Guzmán, F., Martucci, G., Collaud Coen, M., Granados-Muñoz, M. J., Hervo, M., Sicard, M., and Haefele, A.: Characterization of aerosol hygroscopicity using Raman lidar measurements at the EARLINET station of Payerne, Atmospheric Chemistry and Physics, 19, 11 651–11 668, https://doi.org/10.5194/acp-19-11651-2019, 2019.

Ortiz-Amezcua, P., Martínez-Herrera, A., Manninen, A. J., Pentikäinen, P. P., O'Connor, E. J., Guerrero-Rascado, J. L., and Alados-Arboledas, L.: Wind and Turbulence Statistics in the Urban Boundary Layer over a Mountain–Valley System in Granada, Spain, Remote Sensing, 14, https://doi.org/10.3390/rs14102321, 2022.

Pai, S. J., Carter, T. S., Heald, C. L., and Kroll, J. H.: Updated World Health Organization Air Quality Guidelines Highlight the Importance of Non-anthropogenic PM2.5, Environmental Science & Technology Letters, 9, 501–506, https://doi.org/10.1021/acs.estlett.2c00203, 2022.

Pappalardo, G., Amodeo, A., Apituley, A., Comeron, A., Freudenthaler, V., Linné, H., Ansmann, A., Bösenberg, J., D'Amico, G., Mattis, I., et al.: EARLINET: towards an advanced sustainable European aerosol lidar network, Atmospheric Measurement Techniques, 7, 2389–2409, 2014.

Pérez-Ramírez, D., Lyamani, H., Olmo, F. J., Whiteman, D. N., and Alados-Arboledas, L.: Columnar aerosol properties from sun-and-star photometry: statistical comparisons and day-to-night dynamic, Atmospheric Chemistry and Physics, 12, 9719–9738, https://doi.org/10.5194/acp-12-9719-2012, 2012.

Reid, J. S., Eck, T. F., Christopher, S. a., Koppmann, R., Dubovik, O., Eleuterio, D., Holben, B. N., Reid, E. A., and Zhang, J.: A review of biomass burning emissions part III: intensive optical properties of biomass burning particles, Atmospheric Chemistry and Physics, 5, 827–849, 2005.

Román, R., Benavent-Oltra, J., Casquero-Vera, J., Lopatin, A., Cazorla, A., Lyamani, H., Denjean, C., Fuertes, D., Pérez-Ramírez, D., Torres, B., Toledano, C., Dubovik, O., Cachorro, V., de Frutos, A., Olmo, F., and Alados-Arboledas, L.: Retrieval of aerosol profiles combining sunphotometer and ceilometer measurements in GRASP code, Atmospheric Research, 204, 161–177, https://doi.org/https://doi.org/10.1016/j.atmosres.2018.01.021, 2018.

Rosen, J. M., Kjome, N. T., and Oltmans, S. J.: Balloon borne observations of backscatter, frost point and ozone in polar stratospheric clouds at the South Pole, Geophysical Research Letters, 18, 171–174, https://doi.org/https://doi.org/10.1029/90GL02678, 1991.

Sinyuk, A., Holben, B. N., Eck, T. F., Giles, D. M., Slutsker, I., Dubovik, O., Schafer, J. S., Smirnov, A., and Sorokin, M.: Employing relaxed smoothness constraints on imaginary part of refractive index in AERONET aerosol retrieval algorithm, Atmospheric Measurement Techniques, 15, 4135–4151, https://doi.org/10.5194/amt-15-4135-2022, 2022.

Titos, G., Foyo-Moreno, I., Lyamani, H., Querol, X., Alastuey, A., and Alados-Arboledas, L.: Optical properties and chemical composition of aerosol particles at an urban location: An estimation of the aerosol mass scattering and absorption efficiencies, Journal of Geophysical Research: Atmospheres, 117, https://doi.org/https://doi.org/10.1029/2011JD016671, 2012.

Titos, G., Lyamani, H., Pandolfi, M., Alastuey, A., and Alados-Arboledas, L.: Identification of fine (PM1) and coarse (PM10-1) sources of particulate matter in an urban environment, Atmospheric Environment, 89, 593–602, https://doi.org/https://doi.org/10.1016/j.atmosenv.2014.03.001, 2014.

https://doi.org/10.5194/egusphere-2026-990
Preprint. Discussion started: 5 March 2026

Veselovskii, I., Kolgotin, A., Griaznov, V., Müller, D., Wandinger, U., and Whiteman, D. N.: Inversion with regularization for the retrieval of tropospheric aerosol parameters from multiwavelength lidar sounding, Applied optics, 41, 3685–3699, 2002.

Wandinger, U., Freudenthaler, V., Baars, H., Amodeo, A., Engelmann, R., Mattis, I., Groß, S., Pappalardo, G., Giunta, A., D'Amico, G., Chaikovsky, A., Osipenko, F., Slesar, A., Nicolae, D., Belegante, L., Talianu, C., Serikov, I., Linné, H., Jansen, F., Apituley, A., Wilson, K. M., de Graaf, M., Trickl, T., Giehl, H., Adam, M., Comerón, A., Muñoz Porcar, C., Rocadenbosch, F., Sicard, M., Tomás, S., Lange, D., Kumar, D., Pujadas, M., Molero, F., Fernández, A. J., Alados-Arboledas, L., Bravo-Aranda, J. A., Navas-Guzmán, F., Guerrero-Rascado, J. L., Granados-Muñoz, M. J., Preißler, J., Wagner, F., Gausa, M., Grigorov, I., Stoyanov, D., Iarlori, M., Rizi, V., Spinelli, N., Boselli, A., Wang, X., Lo Feudo, T., Perrone, M. R., De Tomasi, F., and Burlizzi, P.: EARLINET instrument intercomparison campaigns: overview on strategy and results, Atmospheric Measurement Techniques, 9, 1001–1023, https://doi.org/10.5194/amt-9-1001-2016, 2016.

Whiteman, D., Melfi, S., and Ferrare, R.: Raman lidar system for the measurement of water vapor and aerosols in the Earth's atmosphere, Applied optics, 31, 3068–3082, 1992.

Whiteman, D., Demoz, B., Rush, K., Schwemmer, G., Gentry, B., Di Girolamo, P., Comer, J., Veselovskii, I., Evans, K., Melfi, S., et al.: Raman lidar measurements during the international H 2 O project. Part I: instrumentation and analysis techniques, Journal of Atmospheric and Oceanic Technology, 23, 157–169, 2006.

Whiteman, D. N., Venable, D., and Landulfo, E.: Comments on "Accuracy of Raman lidar water vapor calibration and its applicability to long-term measurements", Applied Optics, 50, 2170–2176, 2011.

Wiegner, M. and Geiß, A.: Aerosol profiling with the Jenoptik ceilometer CHM15kx, Atmospheric Measurement Techniques, 5, 1953–1964, 2012.

Wiegner, M., Madonna, F., Binietoglou, I., Forkel, R., Gasteiger, J., Geiß, A., Pappalardo, G., Schäfer, K., and Thomas, W.: What is the benefit of ceilometers for aerosol remote sensing? An answer from EARLINET, Atmospheric Measurement Techniques, 7, 1979–1997, https://doi.org/10.5194/amt-7-1979-2014, 2014.